Original Research Article Mathematical modeling and parameter analysis of quantum antenna for IoT sensor-based biomedical applications

Article · August 2023

DOI: 10.32629/jai.v6i2.578

6 authors, including:

Rajveer Yaduvanshi
Nsut

Harendra Singh
G L Bajaj Group of Institutions

Arun Kumar Rana
Galgotias College Of Engineering & Technology

Nitin Goyal
Central University of Haryana

Journal of Autonomous Intelligence (2023) Volume 6 Issue 2
doi:10.32629/jai.v6i2.578

ORIGINAL RESEARCH ARTICLE

Mathematical modeling and parameter analysis of quantum antenna for IoT sensor-based biomedical applications

Ram Krishna[1,2,*], Rajveer Singh Yaduvanshi[3], Harendra Singh[2], Arun Kumar Rana[4], Nitin Goyal[5], Ravinder Kumar[6]

[1] *Department of Electronics and Communication Engineering, Ambedkar Institute of Advanced Communication Technologies and Research (AIACTR), Guru Gobind Indraprastha University (GGSIPU), Delhi 110031, India*

[2] *Department of Electronics and Communication Engineering, G. L. Bajaj Institute of Technology and Management, Greater Noida 201306, India*

[3] *Department of Electronics and Communication Engineering, Netaji Subhas University of Technology (NSUT), Delhi 110078, India*

[4] *Department of Computer Science, Galgotias College of Engineering of Technology, Greater Noida 201310, India*

[5] *Department of Computer Science & Engineering, Central University of Haryana, Mahenderagarh 123031, India*

[6] *Department of Computer Science & Engineering, Shri Vishwakarma Skill University, Palwal 121102, India*

*** Corresponding author:** Ram Krishna, yadavramkrishna@gmail.com

ABSTRACT

In this paper, an equivalent combination of series and parallel R-L-C high-pass filter circuit is derived for a nano (quantum) antenna for the Internet of thing (IoT) based sensors for speedy data or organ image displaying in medical line surgeries. The proposed method utilized the sample frequency behavior of characteristics mode to develop a fundamental building block that superimposes to create the complete response. The resonance frequency, input impedance, and quality factor have been evaluated along with basic and higher-order resonating modes. The relation between quality factor, bandwidth, resonance frequency, and selectivity for higher order, increases the quantum circuits in terms of increased order of a filter, quality factor, and odd and even harmonics factors. Therefore, the basic circuits derivation factor of frequency coefficients are expanded in terms of polynomials and then they are expressed as a simple rational function from which the basic circuit parameters are calculated. In this circuit input impedance of each circuit's element is complex. The real part of input impedance depends on frequency, depending on the frequency positive or negative value of the resistor, and the imaginary part of impedance modelling an inductor or capacitor due to the value of frequency. At cutoff frequency 511 THz, z11 and VSWR parameters are 34 Ω and 1.11, respectively. The proposed quantum DRA is tested at 5 THz, 10 THz, and 500 THz by calculating the electrical parameters like R, L, C and model performance is quite good as compared to existing ones. The dynamic impedance is dependent on the skin effect and enhances the detailed discussion below. The utilization of optical or quantum DRAs is as optical sensors in biomedical engineering, speedy wireless communication, and optical image solutions. Analyte material has been used for monitoring frequency deviation.

Keywords: NDRA (QA); phasor model; resistor; inductor; capacitor; quality factor; dynamic impedance; MATLAB; HFSS software-based simulations

ARTICLE INFO

Received: 30 March, 2023
Accepted: 1 June, 2023
Available online: 9 August, 2023

1. Introduction

The Internet of Things (IoT) is a rapidly growing network of interconnected devices that are designed to communicate with each other and share data. The integration of IoT technology with quantum antennas can result in significant improvements in the performance and efficiency of wireless communication systems[1].

These antennas are designed to operate using the principles of quantum mechanics, which allow for more efficient and precise transmission and reception of signals. Quantum antennas use quantum effects such as entanglement, superposition, and tunneling to enhance their performance and sensitivity. The Internet of Things (IoT) has been rapidly expanding into the healthcare sector and is becoming increasingly important in the monitoring of health conditions. It has the potential to revolutionize disease prevention and help improve patient outcomes. The IoT sensors can be used to monitor various parameters such as temperature, humidity, pressure, and vibration, and transmit this data wirelessly to a central system. The analysis of any antenna and its structure with different parameters has to be known. It involves a large mathematical calculation that can be simplified by its equivalent RLC circuit[3]. In the current article, the HFSS NDRA model has been processed with its electrical equivalent circuit design[4]. An estimated equivalent RLC circuit pattern has been initiated[5] that portrays the principal mode of propagation of the transmission line by utilizing a microstrip coupled slot. Lumped impedances have been attained precisely to narrate the function from source to end terminals. The reactive power due to the inductive and capacitive part is absorbed during excitation and termination while radiated waves are observed by the resistive part only. This methodology can be utilized for computing the input impedance of NDRA with microstrip-coupled loading[6,7]. The designing of NDRA equivalent circuits has been explained in very few research articles, as the maximum part of the research is convenient to the design of equivalent circuits of patch antenna[8–15]. For precise results of internal and load impedance of NDRA, the equivalent circuit representation is essential. The designed parameters of NDRA such as impedances and radiation fields have been represented in higher-order and fundamental resonating modes. Some other parameters like bandwidth, resonating frequency, and radiation field parameters have have been calculated by utilizing an equivalent circuit model[15]. The frequency at which an object vibrates most readily is known as the resonance frequency. It is an object's inherent vibrational frequency. Resonance frequency in electronics refers to the frequency at which a circuit resonates. A resonant circuit is one that may gradually release electrical energy that has been stored in an electric field (capacitor) or magnetic field (inductor). The values of a circuit's components determine its resonance frequency. The design substrate describes the substance used to construct electronic circuits. The substrate supports the circuit mechanically and acts as an electrical insulator between the circuit's several layers. Electric current flowing along a conductor's surface is referred to as surface current[16]. Surface current is significant in electronics because it can lead to unwelcome interference in circuits. By employing appropriate grounding methods and designing circuits with little electromagnetic interference, surface current can be reduced.

In this article, higher-order modes are analyzed exactly. The radiation pattern and the field nature of NDRA[17] can be predicated by resonant modes circuit models. In this research article, a physical science-based circuit for resonant modes has been created straightforwardly in precise structure. It has an advantage analysis and synthesis of distinct NDRA structures. The concept of resonance provides an easier way to design the NDRAs. This analytical approach of linking the Quantum DRA circuit models to its radiated fields is used in NDRA research initially[18–21]. The light beam interacts and passes through the medium that has a collision with fundamental negatively charged particles and molecules of the material[22]. The material medium is considered plasma which possesses the property of explicit permittivity, permeability, and conduction to propagate the EM waves in it at optical frequency.

The integration of IoT technology with quantum antennas has the potential to significantly improve the performance and efficiency of wireless communication systems[23,24]. This can lead to a wide range of applications, including smart cities, healthcare, transportation, and industrial automation. The main motive for to design and analysis of the proposed quantum antenna for wideband (THz) frequency in the biomedical field is to reduce the signal transmission time with low power dissipation. The objectives of the paper are:

1) Understanding the designing analysis of proposed quantum antenna for wideband (THz) frequency in the biomedical field using HFSS microwave studio and MATLAB tools.

2) The proposed quantum antenna provides a wideband (THz) or low wavelength with low power dissipation, therefore, less number of surrounding tissues are damaged when used in biomedical applications.

3) The limitations associated with metals and all-dielectric-based structures antennas can be avoided by utilizing a quantum antenna.

4) The proposed quantum antenna becomes less sensitive toward temperature variations, less expensive, small in size and weight, low wavelength, low power dissipation, and less body tissue damage when used in biomedical applications like laser operations.

The paper is structured as follows: Sections 2 and 3 provide the interpretation and radiation theory related to a quantum antenna. Section 4 discusses the quantum DRA circuit and its analysis. Section 5 discusses the simulated results of the proposed antenna using MATLAB. Section 6 shares the results analysis and response tuning of the proposed antenna using HFSS software. Finally, the paper is concluded in Section 7.

2. Interpretation of quantum antenna

With light amplification and stimulated emission of radiation (LASER) feed, the quantum antenna persists only with dynamic impedance at resonance as the input impedance (Z_i). In this situation, this dynamic impedance depends on the optical frequency and Plank's constant just as the dynamic impedance of classical DRA. With an increment in optical frequency above the resonating frequency (ω_{r2}), the dynamic impedance or the input impedance will be increased which follows the pattern as that of capacitor charging[25–27]. It has been analyzed that the antenna's bandwidth has also been increased with increment in optical frequency but its effect on the quality factor is reversed due to the proposed rectangular shape of a quantum antenna having of larger surface area than other shapes.

In the electrical equivalent circuit of a quantum antenna, the impedance has quite a low value when the frequency is increased highly, so the current I_l maximizes correspondingly, which results in high power and signal strength[28–31]. It also provides very high signal absorption and dispatching. Initially, when the circuit is tuned, the inductive branch current behaves as a surface current that depends on the area. This current is present due to the skin effect. In QA, both impedances (input as well as dynamic) depend on frequency. The actual power is only due to the real part of the input impedance and the non-real part has no contribution in useful power. Both reactive elements (inductor and capacitor) transfer power from one-half cycle to the other half cycle between themselves.

Such types of models are specially required for 5G applications due to very small power loss and high selectivity at larger frequencies[32]. As the inductor or capacitor stores larger power than the dissipated power, therefore the quality factor will be very low, i.e., $Q = \frac{f_r}{bandwidth}$. The quality factor inversely depends on bandwidth, so the bandwidth will be very high. Finally, the bandwidth of an antenna gets improved which allows passing the of high-range signals. The expression of the formula for a resonant frequency of THz NDRA is given by Equation (1)[33].

$$f_r = \frac{c}{2\pi\sqrt{\epsilon_r}}\sqrt{\left(\frac{m\pi}{a}\right)^2 + \left(\frac{n\pi}{b}\right)^2 + \left(\frac{p\pi}{d}\right)^2} \text{ and}$$

$$Q = \frac{f_r}{f_h - f_l} = \frac{f_r}{bandwidth} \tag{1}$$

The terahertz frequency has the advantage of a smaller wavelength. Hence, the depth of signal penetration will be less as compared to microwaves. However, power input level variation results will be different. Terahertz frequency is nonionizing and non-invasive. THz imaging in biological applications is based on the differences in water content and physiological structural changes between abnormal and normal tissues observed. Change in power level may be used to capture images of layered tissue[34]. This

Table 1. Used symbols in mathematical modeling with their nomenclature.

Symbol	Nomenclature
Q	Position vector
P	Time derivative moment vector
β	Temperature
P	Average field energy in Gibb's state
a_k	Annihilation and creation operators
H	Electromagnetic field
$z_q(\beta)$	Quantum partition function
$i(t)$	Current through shunt R-L-C circuit
f_r	Resonant frequency in Hz
BW	Bandwidth
Z	Impedance
P	Power
Z_{in}	Input impedance
Q	Quality factor
Y_1, Y_2, Y_3	Individual admittance of each DRA
R_1, R_2, R_3	Individual Resistance of each branch of DRA
Z_d	Impedance of DRA
Z_L and Z_{in}	DRA load and input impedance
X_1, X_2, X_3	Individual capacitance of each branch of DRA
Y_l	Load admittance
A and B	Real and imaginary parts of the input admittance Y_{in}
$\|S_{11}\|$	Magnitude of the complex reflection coefficient
$\vec{E}_{\varphi s}$	Time-varying field
Z_p	Equivalent impedance of quantum DRA

can have better resolution results as compared to MRI with minimal investment. Terahertz device size shall be very small as compared to MRI. Dielectric behaves like a conductor at high frequency and conductor behaves like a dielectric. Biosafety is an important issue in sensing as the electron energy of the THz wave is low. Biomedical technology (tissue exhibits reflection and absorption properties that change dramatically with tissue characteristics), is used for medical and dental Imaging. Here, it has been demonstrated that the dielectric response of the cell can reflect particular water dynamics by THz spectroscopy. **Table 1** shows the used symbols in mathematical modeling with their Nomenclature.

3. Nano dielectric resonator antenna (NDRA) radiation theory

$$[q_a, p_b] = \frac{ih}{2\pi}\delta(a,\ b) \tag{2}$$

where,

q = Position vector

p = Time derivative moment vector

$\beta = \frac{1}{kT}$, T = Temperature

$\rho = \frac{exp(-\beta H)}{T_r(exp(-\beta H))}$ average field energy in Gibb's state = ρ is explained by $T_r(\rho H)$ and $T_r(\rho p_\epsilon)$. Classically, we get $\frac{\int exp(-\beta H)p_a d^N q d^N p}{\int exp(-\beta H) d_q^N d_p^N} = 0.$

$a_k = \frac{a_k + i\, p_k}{\sqrt{2}}$ annihilation and creation operators $a_k^* = \frac{a_k - ip_k}{\sqrt{2}},\ k = 1, 2, 3 \ldots\ldots\ldots..$

$[a_k, a_m^*] = \frac{h}{2\pi}\delta(k, m)$ Heisenberg commutation relation

Electromagnetic field = $H = \frac{1}{2}\sum_{k=1}^{N} a_k^*\, a_k + \frac{Nh}{4\pi}$ field energy quantum states or eigenstates of $H|\underline{n} \geq n_1, n_2, n_3 \ldots\ldots\ldots\ldots n_N >,\ n_1,\ n_2,\ n_3 \ldots\ldots\ldots. n_N\ = 0, 1, 2, 3 \ldots\ldots$

$H|\underline{n} \geq \frac{h}{2\pi}(\frac{N}{2} + n_1, +n_2 + \cdots \ldots\ldots. n_N)$

Now the Quantum a_k in the Gth state is

$exp\frac{(-\beta Nh)}{4\pi} < n|a_k.exp\left(\frac{(-\beta h)}{2\pi}\sum_m a_m^* a_m\right)(n \geq exp\frac{(-\beta Nh)}{4\pi}\sum_{\underline{n}} exp\left(\frac{(-\beta h)}{2\pi}\sum_m n_m\right)\delta(n, m - e_k) = 0$

Here, $e_k = [0,\ 0, \ldots\ldots\ldots.0,\ 1, \ldots.0]$, $T_r\left(p_k^2 exp(-\beta h)\right) = -\frac{\frac{1}{2}T_r[(p_k^2 + p_k^{*2} - a_k a_k^* - a_k^* a_k)e^{-\beta h}]}{z_q(\beta)}$

$z_q(\beta)$ = Quantam partition function $= \frac{1}{2z_q(\beta)}T_r\left[\left(a_k^* a_k + \frac{h}{4\pi}\right)exp(-\beta h)\right]$

$= \frac{1}{2z_q(\beta)}exp\left(\frac{(-\beta Nh)}{4\pi}\right)\sum_{\underline{n}}\left(n_k + \frac{1}{2}\right)\frac{h}{2\pi}exp\left(-\frac{\beta h}{4\pi}\sum_m n_m\right)$

$\int exp\left(-\beta\sum_k\frac{(a_k^2 + p_k^2)}{2}\right)a_k^2\, d_q^N d_p^N / z_c(\beta)$

where, $z_c(\beta)$ quantum part.

4. Quantum DRA circuit and analysis

Analysis of series and parallel combination of circuit parameters of Quantum DRA has been provided to calculate current $I(t)$, resonating frequency (f_r) impedance (Z), power (P), and bandwidth (BW)[35,36].

NDRA (Nano DRA) impedance (Z_{in})

Equivalent circuits of nano (quantum) antenna.

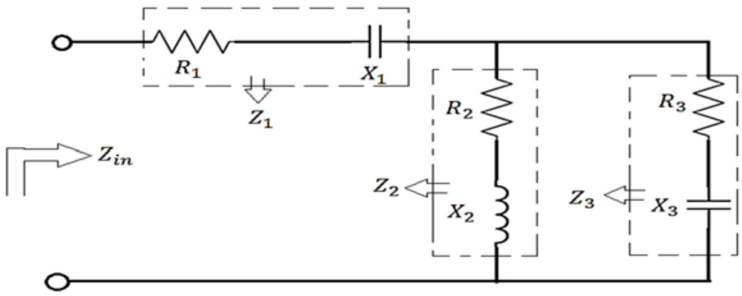

Figure 1. Electrical equivalent impedance circuit of the quantum antenna.

When initial excitation is provided, the voltage drops across the parallel combination of impedance Z_2 and Z_3 is equal and some voltage drop across the impedance Z_1 as shown in **Figure 1**, but the current is divided between impedance Z_2 and Z_3 due to their different values as shown in Equation (3).

$$Z_2 = R_2 + j\omega L_2;\ I_2 = \frac{V}{Z_2} \text{ and } Z_3 = R_3 - \frac{j}{\omega C_3},\ I_3 = \frac{V}{Z_3} \tag{3}$$

The value of Z_2 and Z_3 changes due to variable frequency terms in Z_2 and Z_3. The value of impedance Z_2 and Z_3 will be equal at a particularly high frequency which results in equal current flow. But it remains equal for a very short instant as it persists only for a particular high frequency. The occurrence of this incident is due to the Dirac-delta function. The frequency at which equal current is observed in parallel impedances Z_2 and Z_3 is known as a first tuning frequency. But at this time, the currents I_2 and I_3 in impedance Z_2 and Z_3 individually have equal magnitude but opposite phases to each other. So, its resultant will be zero and the all-current flows through the impedance Z_1 alone, which is expressed as $Z_1 = R_1 - \frac{j}{\omega C_1}$ (Z_1 is frequency dependent)[37]. When the frequency gets higher, the value of the impedance Z_1 is decreased to a low value which results in a huge amount of current and power. Under this condition, Z_1 is considered as a dynamic impedance of the circuit as the impedance depends only on Z_1. This impedance depends on the frequency and having characteristics of exponentially increased function similar to the charging of a capacitor. The current in Z_1 depends on a voltage drop across Z_1 and given by $i_i = C\frac{dV_1}{dt}$ as dt is quite small, so the higher current results in large bandwidth. This current i_i is called as surface or displacement current.

In **Figure 1**, $X_1 = -\frac{1}{\omega C_1}$, $X_2 = \omega L_2$ and $X_3 = -\frac{1}{\omega C_3}$.

Input impedance $Z_{in} = Z_1 + Z_2 \| Z_3 = Z_1 + \frac{Z_2 Z_3}{Z_2 + Z_3}$

where,

$Z_1 = R_1 + jX_1$, $Z_2 = R_2 + jX_2$ and $Z_3 = R_3 + jX_3$

$$Z_{in} = R_1 + jX_1 + \frac{(R_3 + jX_3)(R_2 + jX_2)}{R_2 + jX_2 + R_3 + jX_3} = R_1 + jX_1 + \frac{R_2R_3 - X_2X_3 + j(X_2R_3 + R_2X_3)}{R_2 + R_3 + j(X_3 + X_2)}$$

$$= R_1 + jX_1 + \frac{(R_2R_3 - X_2X_3)(R_2 + R_3) + (X_2R_3 + R_2X_3)(X_3 + X_2) + j\{(R_2 + R_3)(X_2R_3 + R_2X_3) - (X_3 + X_2)(R_2R_3 - X_2X_3)\}}{(R_2 + R_3)^2 + (X_3 + X_2)^2}$$

$$Z_{in}(\text{real part}) = \left[R_1 + \frac{(R_2R_3 - X_2X_3)(R_2 + R_3) + (X_2R_3 + R_2X_3)(X_3 + X_2)}{(R_2 + R_3)^2 + (X_3 + X_2)^2}\right] \tag{4}$$

$$Z_{in}(\text{imaginary part}) = \left[X_1 + \frac{(R_2+R_3)(X_2R_3+R_2X_3)-(X_3+X_2)(R_2R_3-X_2X_3)}{(R_2+R_3)^2+(X_3+X_2)^2}\right] \quad (5)$$

To obtain the resonance condition, the imaginary part of an input impedance must be zero[38]. $Z_{in} = Z_{in}(\text{real part}) + Z_{in}(\text{imaginary part})$.

At resonance frequency imaginary part of $Z_{in} = 0$,

$X_1 + \frac{(R_2+R_3)(X_2R_3+R_2X_3)-(X_3+X_2)(R_2R_3-X_2X_3)}{(R_2+R_3)^2+(X_3+X_2)^2} = 0$,

$R_2R_3X_2 + R_2^2X_3 + R_3^2X_2 + R_2R_3X_3 - (R_2R_3X_2 - X_2^2X_3 + R_2R_3X_3 - X_3^2X_2) + X_1\{(R_2+R_3)^2 + (X_3+X_2)^2\} = 0$,

$R_2^2X_3 + R_3^2X_2 + X_2^2X_3 + X_3^2X_2 + X_1(R_2^2 + R_3^2 + 2R_2R_3 + X_2^2 + X_3^2 + 2X_2X_3) = 0$,

$R_2^2(X_1+X_3) + R_3^2(X_1+X_2) + X_2^2(X_1+X_3) + X_3^2(X_1+X_2) + 2X_1(R_2R_3 + X_2X_3) = 0$,

$(R_2^2 + X_2^2)(X_1+X_3) + (R_3^2+X_3^2)(X_1+X_2) + 2X_1(R_2R_3+X_2X_3) = 0$.

Putting the value of X_1, X_2 and X_3.

$$\left(\omega L_2 - \frac{1}{\omega C_1}\right)\left(R_3^2 + \frac{1}{\omega^2C_3^2}\right) + \left(-\frac{1}{\omega C_1} - \frac{1}{\omega C_3}\right)(R_2^2 + \omega^2L_2^2) - \frac{2}{\omega C_1}\left(R_2R_3 - \frac{L_2}{C_3}\right) = 0$$

$$\left(\frac{\omega^2L_2C_1 - 1}{\omega C_1}\right)\left(\frac{R_3^2\omega^2C_3^2+1}{\omega^2C_3^2}\right) + \frac{1}{\omega}\left(-\frac{1}{C_1} - \frac{1}{C_3}\right)(R_2^2 + \omega^2L_2^2) - \frac{2}{\omega C_1}\left(R_2R_3 - \frac{L_2}{C_3}\right) = 0$$

Multiplying ω^3 both sides in the above equation:

$$\frac{(\omega^2L_2C_1-1)(R_3^2\omega^2C_3^2+1)}{C_1C_3^2} + \omega^2\left(-\frac{1}{C_1} - \frac{1}{C_3}\right)(R_2^2+\omega^2L_2^2) - \frac{2\omega^2}{C_1}\left(R_2R_3 - \frac{L_2}{C_3}\right) = 0$$

$$\frac{\left(\omega^4L_2C_1R_3^2C_3^2 - 1 + \omega^2(L_2C_1 - R_3^2C_3^2)\right)}{C_1C_3^2} + \omega^4L_2^2\left(-\frac{1}{C_1} - \frac{1}{C_3}\right) + \omega^2R_2^2\left(-\frac{1}{C_1} - \frac{1}{C_3}\right) - \frac{2\omega^2}{C_1}\left(R_2R_3 - \frac{L_2}{C_3}\right) = 0$$

$$\omega^4\left[L_2R_3^2 - L_2^2\left(\frac{1}{C_1} + \frac{1}{C_3}\right)\right] + \omega^2\left[\frac{L_2}{C_3^2} - \frac{R_3^2}{C_1} - R_2^2\left(\frac{1}{C_1} + \frac{1}{C_3}\right) - \frac{2}{C_1}\left(R_2R_3 - \frac{L_2}{C_3}\right)\right] - \frac{1}{C_1C_3^2} = 0$$

$$\omega^4[A] + \omega^2[B] - C = 0$$

Comparing the above two equations after this where *A*, *B*, and *C* are: $A = L_2R_3^2 - L_2^2\left(\frac{1}{C_1} + \frac{1}{C_3}\right)$, $B = \frac{L_2}{C_3^2} - \frac{R_3^2}{C_1} - R_2^2\left(\frac{1}{C_1} + \frac{1}{C_3}\right) - \frac{2}{C_1}\left(R_2R_3 - \frac{L_2}{C_3}\right)$, and $C = \frac{1}{C_1C_3^2}$, Solution of this equation we assume $\omega^2 = p$, $p^2[A] + p[B] - C = 0, P = \frac{-B\pm\sqrt{B^2+4AC}}{2A}$ where $\omega^2 = p$, $\omega = \sqrt{\frac{-B\pm\sqrt{B^2+4AC}}{2A}}$

$$= \sqrt{\frac{-\left(\frac{L_2}{C_3^2} - \frac{R_3^2}{C_1} - R_2^2\left(\frac{1}{C_1}+\frac{1}{C_3}\right) - \frac{2}{C_1}\left(R_2R_3 - \frac{L_2}{C_3}\right)\right) \pm \sqrt{\left(\frac{L_2}{C_3^2} - \frac{R_3^2}{C_1} - R_2^2\left(\frac{1}{C_1}+\frac{1}{C_3}\right) - \frac{2}{C_1}\left(R_2R_3 - \frac{L_2}{C_3}\right)\right)^2 + 4\left\{L_2R_3^2 - L_2^2\left(\frac{1}{C_1}+\frac{1}{C_3}\right)\right\}\frac{1}{C_1C_3^2}}}{2\left\{L_2R_3^2 - L_2^2\left(\frac{1}{C_1}+\frac{1}{C_3}\right)\right\}}} \quad (6)$$

.

.

The derived formula of input impedance shows its dependency on circuit parameters such as resistance, inductance, capacitance, and resonating frequency[39].

$$Z_{in} = f(R, L, C, \omega)$$

$$Z_{in} = Z_{in\ real}(\omega) + Z_{in\ imaginary}(\omega) \tag{7}$$

In dynamic resonator antenna (DRA), the non-imaginary part of the impedance is independent of frequency so the input impedance can be written as:

$$Z_{in} = Z_{in\ real} + Z_{in\ imaginary}(\omega)$$

$$Z_{in\ real} \neq f(\omega)$$

$Z_{in\ real}$ implies the real part of input impedance alone.

But in NDRA (QA), the real part is frequency dependent that can be given as: $Z_{in\ real}$ = resistance = $f(\omega)$.

This frequency-dependent resistance is additionally referred to as a dynamic resistance of the circuit[40].

$$Z_d = R_1 + \frac{(R_2R_3 - X_2X_3)(R_2 + R_3) + (X_2R_3 + R_2X_3)(X_3 + X_2)}{(R_2 + R_3)^2 + (X_3 + X_2)^2} \tag{8}$$

Putting the value of $X_1 = \frac{1}{-\omega C_1}$, $X_2 = \omega C_2$ and $X_3 = \frac{1}{-\omega C_3}$ in above equation:

$$Z_d = R_1 + \frac{\left(R_2R_3 - \frac{L_2}{C_3}\right)(R_2 + R_3) + \left(\omega L_2 R_3 - \frac{R_2}{\omega C_3}\right)\left(\omega L_2 - \frac{1}{\omega C_3}\right)}{(R_2 + R_3)^2 + \left(\omega L_2 - \frac{1}{\omega C_3}\right)^2}$$

$$Z_d = R_1 + \frac{\left(R_2R_3 - \frac{L_2}{C_3}\right)(R_2 + R_3) + \left(\frac{\omega^2 L_2 R_3 C_3 - R_2}{\omega C_3}\right)\left(\frac{\omega^2 L_2 C_3 - 1}{\omega C_3}\right)}{(R_2 + R_3)^2 + \left(\frac{\omega^2 L_2 C_3 - 1}{\omega C_3}\right)^2}$$

$$Z_d = R_1 + \frac{\frac{\left(R_2R_3 - \frac{L_2}{C_3}\right)(R_2 + R_3)\omega^2 C_3^2 + (\omega^2 L_2 R_3 C_3 - R_2)(\omega^2 L_2 C_3 - 1)}{\omega^2 C_3^2}}{\frac{\omega^2 C_3^2 (R_2 + R_3)^2 + (\omega^2 L_2 C_3 - 1)^2}{\omega^2 C_3^2}}$$

$$Z_d = \frac{R_1\left\{\omega^2 C_3^2 (R_2 + R_3)^2 + (\omega^2 L_2 C_3 - 1)^2\right\} + \left(R_2R_3 - \frac{L_2}{C_3}\right)(R_2 + R_3)\omega^2 C_3^2 + (\omega^2 L_2 R_3 C_3 - R_2)(\omega^2 L_2 C_3 - 1)}{\omega^2 C_3^2 (R_2 + R_3)^2 + (\omega^2 L_2 C_3 - 1)^2} \tag{9}$$

$$Z_d = f(\omega) \text{ or } R_{in} = f(\omega)$$

In the alternative method, there are two resonant mode presents in this circuit. In another way to explain in the below circuit.

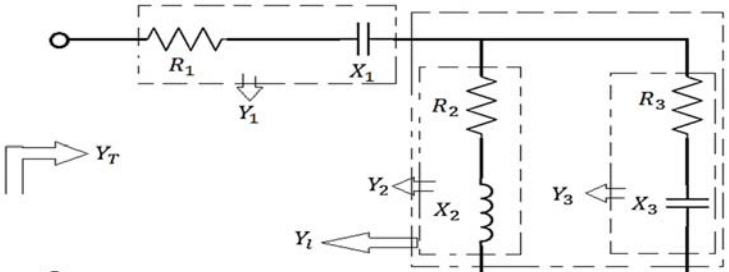

Figure 2. Electrical equivalent admittance circuit of a quantum antenna.

$$X_1 = -\frac{1}{\omega C_1}, X_2 = \omega L_2 \text{ and } X_3 = -\frac{1}{\omega C_3}$$

$$Y_l = Y_2 + Y_3, Y_l = \frac{1}{R_2 + jX_2} + \frac{1}{R_3 + jX_3}$$

$$Y_l = \frac{1}{R_2 + j\omega L_2} + \frac{1}{R_3 - \frac{j}{\omega C_3}}, Y_l = \frac{R_2 - j\omega L_2}{R_2 + j\omega L_2} + \frac{R_3 + \frac{j}{\omega C_3}}{R_3 - \frac{j}{\omega C_3}}$$

$$Y_l = \frac{R_2}{R_2^2 + \omega^2 L_2^2} + \frac{R_3}{R_3^2 + \frac{1}{\omega^2 C_3^2}} + j\left[\frac{\frac{1}{\omega C_3}}{R_3^2 + \frac{1}{\omega^2 C_3^2}} - \frac{\omega L_2}{R_2^2 + \omega^2 L_2^2}\right] \tag{10}$$

$$Y_l = G_l + jB_l$$

For the first resonating mode susceptance (imaginary part) of $(Y_l) = 0$, i.e., $B_l = 0$

$$\frac{\frac{1}{\omega C_3}}{R_3^2 + \frac{1}{\omega^2 C_3^2}} - \frac{\omega L_2}{R_2^2 + \omega^2 L_2^2} = 0, \frac{\frac{1}{\omega C_3}}{R_3^2 + \frac{1}{\omega^2 C_3^2}} = \frac{\omega L_2}{R_2^2 + \omega^2 L_2^2}$$

$$\frac{\omega C_3}{R_3^2 \omega^2 C_3^2 + 1} = \frac{\omega L_2}{R_2^2 + \omega^2 L_2^2}, C_3(R_2^2 + \omega^2 L_2^2) = L_2(R_3^2 \omega^2 C_3^2 + 1)$$

$$\omega^2(L_2^2 C_3 - L_2 R_3^2 C_3^2) = L_2 + R_2^2 C_3$$

$$\omega = \sqrt{\frac{L_2 + R_2^2 C_3}{L_2^2 C_3 - L_2 R_3^2 C_3^2}} \tag{11}$$

For the second resonant mode of this circuit,

$$Y_T = Y_1 + Y_l, Y_T = Y_1 + (G_l + jB_l)$$

$$Y_T = \frac{1}{R_1 - \frac{j}{\omega C_1}} + (G_l + jB_l), Y_T = \frac{R_1 + \frac{j}{\omega C_1}}{R_1^2 + \frac{1}{\omega^2 C_1^2}} + (G_l + jB_l)$$

$$Y_T = \left(\frac{R_1 \omega^2 C_1^2}{R_1^2 \omega^2 C_1^2 + 1} + G_l\right) + j\left(B_l + \frac{\frac{1}{\omega C_1}}{R_1^2 + \frac{1}{\omega^2 C_1^2}}\right)$$

To achieve second resonating mode, the imaginary part of $Y_T = 0$, $B_l + \frac{\omega C_1}{R_1^2 \omega^2 C_1^2 + 1} = 0$

$$\frac{\omega C_3}{R_3^2 \omega^2 C_3^2 + 1} - \frac{\omega L_2}{R_2^2 + \omega^2 L_2^2} + \frac{\omega C_1}{R_1^2 \omega^2 C_1^2 + 1} = 0, \frac{C_3}{R_3^2 \omega^2 C_3^2 + 1} - \frac{L_2}{R_2^2 + \omega^2 L_2^2} + \frac{C_1}{R_1^2 \omega^2 C_1^2 + 1} = 0$$

After solving this equation, the value of ω_r

$$\omega r = \sqrt{\frac{-\left(\frac{L_2}{C_3^2} - \frac{R_3^2}{C_1} - R_2^2\left(\frac{1}{C_1} + \frac{1}{C_3}\right) - \frac{2}{C_1}\left(R_2 R_3 - \frac{L_2}{C_3}\right)\right) \pm \sqrt{\left(\frac{L_2}{C_3^2} - \frac{R_3^2}{C_1} - R_2^2\left(\frac{1}{C_1} + \frac{1}{C_3}\right) - \frac{2}{C_1}\left(R_2 R_3 - \frac{L_2}{C_3}\right)\right)^2 + 4\left\{L_2 R_3^2 - L_2^2\left(\frac{1}{C_1} + \frac{1}{C_3}\right)\right\}\frac{1}{C_1 C_3^2}}}{2\left\{L_2 R_3^2 - L_2^2\left(\frac{1}{C_1} + \frac{1}{C_3}\right)\right\}}} \tag{12}$$

.
.

Quality factor (Q) = $2\pi \times \frac{\text{maximum energy stored per cycle}}{\text{power dissipated per cycle}}$.

To analyze series circuit: $Z = R + jX$…….$= R + j(X_L - X_C)$…, Q $= \frac{|X_L|}{R} = \frac{|X_C|}{R}$….

But for analysis of parallel circuit, $Y = G + jB = G + j(B_c - B_L)$, Q $= \frac{|B_L|}{G} = \frac{|B_C|}{G}$. According to this,

$$Z_{in} = R_{in} + jX_{in} = Z_{in}(real) + Z_{in}(imaginary)$$

$$\text{Quality factor } (Q) = \left| \frac{\frac{R_2^2 X_3 + X_2^2 X_3}{(R_2+R_3)^2+(X_3+X_2)^2}}{R_1 + \frac{(R_2R_3 - X_2X_3)(R_2+R_3)+(X_2R_3+R_2X_3)(X_3+X_2)}{(R_2+R_3)^2+(X_3+X_2)^2}} \right| \tag{13}$$

$$Q = \frac{R_2^2 X_3 + X_2^2 X_3}{(R_2R_3 - X_2X_3)(R_2+R_3)+(X_2R_3+R_2X_3)(X_3+X_2)+R_1\{(R_2+R_3)^2+(X_3+X_2)^2\}}$$

$$Q = \frac{\mathrm{R_2^2X_3+X_2^2X_3}}{\mathrm{R_2^2R_3+R_3^2R_2-R_2X_2X_3-X_2R_3X_3-\left(X_2^2R_3+X_3^2R_2+X_2X_3R_2+X_2X_3R_3\right)+R_1\left\{R_2^2+R_3^2+2R_2R_3+X_2^2+X_3^2+2X_2X_3\right\}}}$$

$$Q = \frac{R_2^2 X_3 + X_2^2 X_3}{R_2^2(R_3+R_1)+R_3^2(R_2+R_1)+X_2^2(R_3+R_1)+X_3^2(R_2+R_1)+2R_1(R_2R_3+X_2X_3)-2X_2X_3R_2-2X_2X_3R_3}$$

$$Q = \frac{R_2^2 X_3 + X_2^2 X_3}{(R_3+R_1)\left(R_2^2+X_2^2\right)+(R_2+R_1)\left(R_3^2+X_3^2\right)+2R_2(R_1R_3-X_2X_3)+2X_2(X_3R_1-X_3R_3)}$$

$$Q = \frac{-R_2^2\frac{1}{\omega C_3}-\omega^2L_2^2\frac{1}{\omega C_3}}{(R_3+R_1)\left(R_2^2+\omega^2L_2^2\right)+(R_2+R_1)\left(R_3^2+\frac{1}{\omega^2C_3^2}\right)+2R_2\left(R_1R_3-\frac{L_2}{C_3}\right)+2\omega L_2\left(\frac{-R_1}{\omega C_1}+\frac{R_3}{\omega C_3}\right)}$$

$$Q = \frac{-R_2^2\frac{1}{\omega C_3}-\omega^2L_2^2\frac{1}{\omega C_3}}{(R_3+R_1)\left(R_2^2+\omega^2L_2^2\right)+(R_2+R_1)\left(\frac{\omega^2C_3^2R_3^2+1}{\omega^2C_3^2}\right)+2R_2\left(R_1R_3-\frac{L_2}{C_3}\right)+2L_2\left(\frac{-R_1}{C_1}+\frac{R_3}{C_3}\right)}$$

Multiplying ω^2 numerator and denominator:

$$Q = \frac{-\omega\frac{R_2^2}{C_3}-\omega^3\frac{L_2^2}{C_3}}{\omega^2(R_3+R_1)\left(R_2^2+\omega^2L_2^2\right)+\left(\frac{R_2+R_1}{C_3^2}\right)\left(\omega^2C_3^2R_3^2+1\right)+2\omega^2R_2\left(R_1R_3-\frac{L_2}{C_3}\right)+2\omega^2L_2\left(\frac{-R_1}{C_1}+\frac{R_3}{C_3}\right)}$$

$$\text{Quality factor } (Q) = \left| \frac{-\omega^3\frac{L_2^2}{C_3}-\omega\frac{R_2^2}{C_3}}{\omega^4\left[L_2^2(R_3+R_1)\right]+\omega^2\left[R_2^2(R_3+R_1)+R_3^2(R_2+R_1)+2R_2\left(R_1R_3-\frac{L_2}{C_3}\right)+2L_2\left(\frac{-R_1}{C_1}+\frac{R_3}{C_3}\right)\right]+\left[\frac{R_2+R_1}{C_3^2}\right]} \right| \tag{14}$$

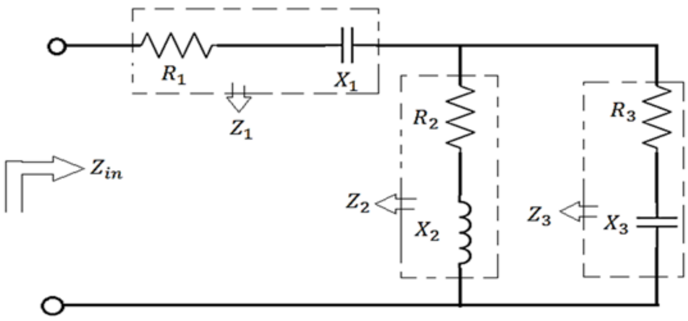

Figure 3. Electrical equivalent impedance circuit of quantum antenna for phasor representation.

The phasor representation of equivalent circuit of QA (**Figure 3**) is shown in **Figure 4**.

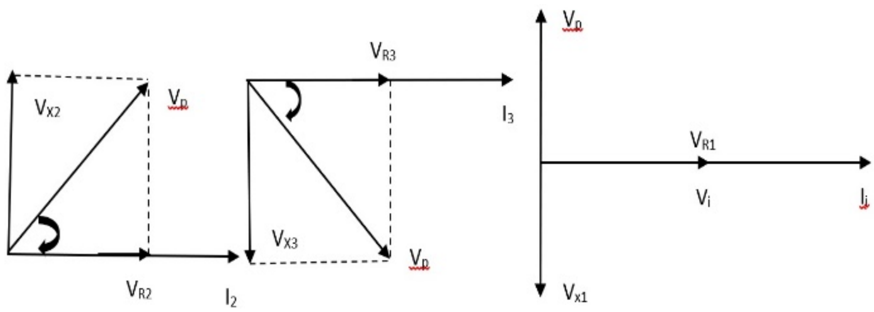

Figure 4. Phasor diagram of an electrical equivalent circuit of the quantum antenna.

$$V_{R_2} = I_2R_2 = I_2R_2 \angle 0^0, V_{X_2} = I_2X_2 = I_2\omega L_2 \angle 90^0$$

$$V_P = \sqrt{V_{R_2}^2 + V_{X_2}^2}, V_{R_3} = I_3 R_3 = I_3 R_3 \angle 0^0$$

$$V_{X_3} = I_3 X_3 = \frac{I_3}{\omega C_3} \angle -90^0, V_P = \sqrt{V_{R_3}^2 + V_{X_3}^2}$$

For the parallel combination $V_{PZ_2} = V_{PZ_3}$,

$$\sqrt{V_{R_2}^2 + V_{X_2}^2} = \sqrt{V_{R_3}^2 + V_{X_3}^2}, \sqrt{I_2^2 R_2^2 + I_2^2 X_2^2} = \sqrt{I_3^2 R_3^2 + I_3^2 X_3^2}$$

$$I_2 \sqrt{R_2^2 + X_2^2} = I_3 \sqrt{R_3^2 + X_3^2}, I_2 \sqrt{R_2^2 + \omega^2 L_2^2} = I_3 \sqrt{R_3^2 + \frac{1}{\omega^2 C_3^2}}$$

At the resonance mode $|I_2| = |I_3|$ and squaring both sides,

$$R_2^2 + \omega^2 L_2^2 = R_3^2 + \frac{1}{\omega^2 C_3^2}, \omega_{r1}^4 L_2^2 C_3^2 - (R_2^2 - R_3^2)\omega_{r1}^2 C_3^2 + 1 = 0$$

$$\omega_{r1} = \sqrt{\frac{(R_2^2 - R_3^2)C_3^2 \pm \sqrt{(R_2^2 - R_3^2)^2 C_3^4 - 4L_2^2 C_3^2}}{2L_2^2 C_3^2}}$$

By solving the parallel impedances Z_2 and Z_3 into an equivalent impedance Z_P, **Figure 3** can be represented as shown in **Figure 5**.

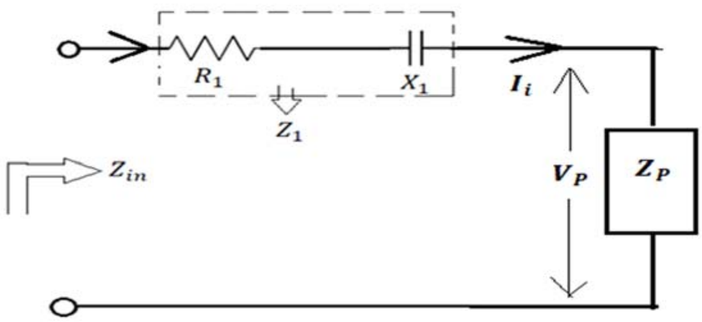

Figure 5. Modified electrical equivalent impedance circuit of a quantum antenna.

$$V_i = V_1 - V_p, V_{R_1} = I_i R_1 = I_i R_1 \angle 0^0$$

$$V_{X_1} = I_i X_1 = I_i \frac{1}{\omega C_1} \angle -90^0, V_P = I_i Z_P = I_i Z_P \angle 90^0$$

At the particular frequency, $V_{Z_1} = V_P$ and arises another mode of resonance frequency:

$$I_i Z_P = I_i Z_1, Z_P = Z_1, \frac{1}{Y_1 + Y_2} = Z_1$$

After this solution of resonance frequency:

$$\omega_{r2} = \sqrt{\frac{-\left(\frac{L_2}{C_3^2} - \frac{R_3^2}{C_1} - R_2^2\left(\frac{1}{C_1} + \frac{1}{C_3}\right) - \frac{2}{C_1}\left(R_2 R_3 - \frac{L_2}{C_3}\right)\right) \pm \sqrt{\left(\frac{L_2}{C_3^2} - \frac{R_3^2}{C_1} - R_2^2\left(\frac{1}{C_1} + \frac{1}{C_3}\right) - \frac{2}{C_1}\left(R_2 R_3 - \frac{L_2}{C_3}\right)\right)^2 + 4\left\{L_2 R_3^2 - L_2^2\left(\frac{1}{C_1} + \frac{1}{C_3}\right)\right\}\frac{1}{C_1 C_3^2}}}{2\left\{L_2 R_3^2 - L_2^2\left(\frac{1}{C_1} + \frac{1}{C_3}\right)\right\}}}$$

$$Z_{in} = Z_1 + Z_P, Z_{in} = Z_1 + \frac{1}{Y_P} = Z_1 + \frac{1}{Y_2+Y_3}$$

$$Z_{in} = R_1 + JX_1 + \frac{1}{Y_P} = R_1 + JX_1 + \frac{1}{\frac{1}{R_2+JX_2} + \frac{1}{R_3+JX_3}}$$

$$Z_{in} = R_1 + JX_1 + \frac{1}{Y_P} = R_1 + JX_1 + \frac{1}{\frac{R_2-JX_2}{R_2^2+X_2^2} + \frac{R_3-JX_3}{R_3^2+X_3^2}}$$

$$Z_{in} = R_1 + JX_1 + \frac{1}{Y_P} = R_1 + JX_1 + \frac{1}{\frac{R_2}{R_2^2+X_2^2} + \frac{R_3}{R_3^2+X_3^2} - J\left(\frac{X_2}{R_2^2+X_2^2} + \frac{X_3}{R_3^2+X_3^2}\right)}$$

$$Z_{in} = R_1 + JX_1 + \frac{1}{Y_P} = R_1 + JX_1 + \frac{1}{A - JB}$$

where,

$$A = \frac{R_2}{R_2^2+X_2^2} + \frac{R_3}{R_3^2+X_3^2} \text{ and } B = \frac{X_2}{R_2^2+X_2^2} + \frac{X_3}{R_3^2+X_3^2}$$

$$Z_{in} = R_1 + JX_1 + \frac{1}{Y_P} = R_1 + JX_1 + \frac{A+JB}{A^2+B^2}$$

$$Z_{in} = R_1 + \frac{A}{A^2+B^2} + J\left(X_1 + \frac{B}{A^2+B^2}\right) = Z_{inr} + Z_{inima}$$

The classical DRA can be analyzed by its equivalent series RLC circuit[41]. The research done till now explains that the dynamic electrical concept of classical DRA is freelance from an operational frequency in the range of microwave spectrum and planks constant. But the laser-fed quantum antenna doesn't have such type of observations. The formulation and calculation of dynamic impedance of QA the above observations are analyzed through mathematical reduction and simulation in HFSS software for its modeling. The shunt branch impedance Z_2 and Z_3 are tuned to take it in an optical frequency range such that where $|Z_2| = |Z_3|$, the resonance condition is obtained but both of these impedances are in opposite phases. So, the whole circuit of a quantum antenna can be represented by impedance Z_1 which is a series combination of resistor and capacitor. As the angular resonant frequency depends on the values of inductance and capacitance ($\omega_{r1} \propto \frac{1}{L_2 C_3}$). Thus, by changing their values, we can modify the bandwidth of the circuit. If there is a further increment in the value of ω_{r1} the quantum antenna circuit reacts as a series combination RLC[42]. So, it is obvious that another resonant frequency (ω_{r2}) is achieved due to the tuning between Z_1 and the resultant of parallel impedance ZP that is a parallel combination of Z_2 anf Z_3.

The expression of (ω_{r2}) shows that there is an effect of the values of R_2, R_3, L_2, C_1, and C_3 on it. But, the foremost impact on (ω_{r2}) is of the value of C_1. So, if C_1 is increased, the resonating frequency ω_{r2} would increase accordingly.

The nano-antenna circuit acts as a filter due to zero circuit output for a domain of frequency and finite output for a specific range of frequency[43]. So, there is existence 1 stage 2 mode only in a nano-antenna circuit. However, for the higher stage, odd and even harmonics of ω will be increased.

For the primary stage of the filter, 1st and 2nd mode resonating parameters such as f_r are calculated. Considering **Figure 6**, the input excitation and output response are represented by X_i and X_o.

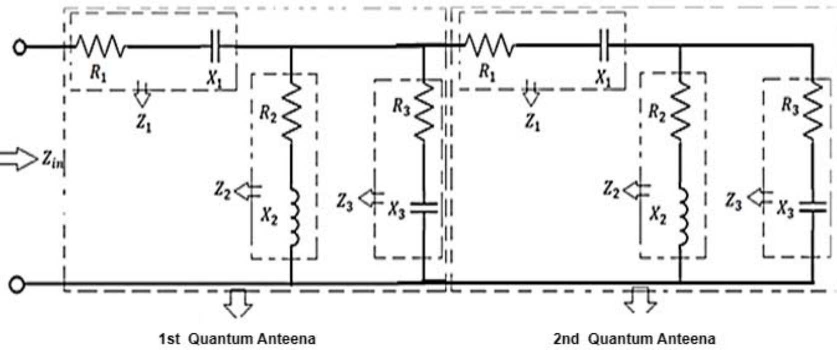

Figure 6. 6th order quantum antenna (multistage quantum antenna).

Applying the Laplace transform $Z_1 = \frac{R_1 sC_1+1}{sC_1}$, $Z_2 = R_2 + sL_2$ and $Z_3 = \frac{R_3 sC_3+1}{sC_3}$

$$\frac{X_o(s)}{X_i(s)} = \frac{Z_p}{Z_1+Z_p} = \frac{Z_2 Z_3}{Z_1(Z_2+Z_3)+Z_2 Z_3}$$

where,

$$Z_p = \frac{Z_2 Z_3}{(Z_2+Z_3)}$$

$$\frac{X_o(s)}{X_i(s)} = \frac{1}{1+\frac{Z_1}{Z_p}} = \frac{1}{1+\frac{\frac{R_1 sC_1+1}{sC_1}}{\frac{(R_2+sL_2)\left(\frac{R_3 sC_3+1}{sC_3}\right)}{(R_2+R_3+sL_2)sC_3+1}}} = \frac{1}{1+\frac{(R_1 sC_1+1)\{(R_2+R_3+sL_2)sC_3+1\}}{sC_1(R_2+sL_2)(R_3 sC_3+1)}}$$

$$\frac{X_o(s)}{X_i(s)} = \frac{1}{1+\frac{s^3 R_1 C_1 L_2 C_3 + s^2\{L_2 C_3 + R_1 C_1 C_3 (R_2+R_3)\} + R_1 C_1 s + 1}{s^3 R_3 C_1 L_2 C_3 + s^2 (L_2 C_3 + R_2 R_3 C_1 C_3) + R_2 C_1 s}} \quad (15)$$

Put $s = j\omega$, the transfer function will be:

$$\frac{X_o(j\omega)}{X_i(j\omega)} = \frac{1}{1+\frac{1-\omega^2\{L_2 C_3 + R_1 C_1 C_3 (R_2+R_3)\} + j(R_1 C_1 \omega - \omega^3 R_1 C_1 L_2 C_3)}{-\omega^2 (L_2 C_3 + R_2 R_3 C_1 C_3) + j(\omega R_2 C_1 - \omega^3 R_3 C_1 L_2 C_3)}} \quad (16)$$

The characteristics and behavior of QA as the acceptor or rejector circuit are described by Equation (14). It behaves as an acceptor circuit (band-pass filter) and a rejector circuit (band rejects filter)[44].

Different operating modes can be calculated by simplifying the transfer function as:

$$\frac{X_o(j\omega)}{X_i(j\omega)} = \frac{1}{1+\frac{a+jb}{c+jc}} = \frac{1}{1+\frac{a+c+j(b-d)}{c^2+d^2}}$$

where,

$$a = 1 - \omega^2\{L_2 C_3 + R_1 C_1 C_3 (R_2+R_3)\}$$

$$b = R_1 C_1 \omega - \omega^3 R_1 C_1 L_2 C_3$$

$$c = -\omega^2 (L_2 C_3 + R_2 R_3 C_1 C_3)$$

$$d = (\omega R_2 C_1 - \omega^3 R_3 C_1 L_2 C_3)$$

$$\left|\frac{X_o(j\omega)}{X_i(j\omega)}\right| = \frac{1}{\sqrt{\left(1+\frac{a+c}{c^2+d^2}\right)^2 + \left(\frac{b-d)}{c^2+d^2}\right)^2}}$$

At high response of transfer function $b - d = 0$ and $a + c = 0$

Applying this condition, there will be two modes generated at different frequencies

$$(R_1C_1\omega - \omega^3 R_1C_1L_2C_3) - (\omega R_2C_1 - \omega^3 R_3C_1L_2C_3) = 0$$

And the 2nd condition is

$$1 - \omega^2\{L_2C_3 + R_1C_1C_3(R_2 + R_3)\} - \omega^2(L_2C_3 + R_2R_3C_1C_3) = 0$$

$$\omega_1 = \sqrt{\frac{R_1C_1 - R_2C_1}{R_1C_1L_2C_3 - R_3C_1L_2C_3}} \tag{17}$$

$$\omega_2 = \sqrt{\frac{1}{L_2C_3 + R_2R_3C_1C_3 + \{L_2C_3 + R_1C_1C_3(R_2 + R_3)\}}} \tag{18}$$

The bandwidth of nano-antenna:

$$(\mathrm{BW}) = (\omega_2 - \omega_1) = \sqrt{\frac{1}{L_2C_3+R_2R_3C_1C_3+\{L_2C_3+R_1C_1C_3(R_2+R_3)\}}} - \sqrt{\frac{R_1C_1-R_2C_1}{R_1C_1L_2C_3-R_3C_1L_2C_3}} \tag{19}$$

As per the above discussion, the input impedance is only the function of the non-imaginary part of Z_{in} and that non-imaginary part is frequency dependent[45–49]. This relation implies the quality factor as

$$Q = \frac{\omega_r}{(\omega_2-\omega_1)} = \frac{\sqrt{\dfrac{-\left(\frac{L_2}{C_3^2}-\frac{R_3^2}{C_1}-R_2^2\left(\frac{1}{C_1}+\frac{1}{C_3}\right)-\frac{2}{C_1}\left(R_2R_3-\frac{L_2}{C_3}\right)\right)\pm\sqrt{\left(\frac{L_2}{C_3^2}-\frac{R_3^2}{C_1}-R_2^2\left(\frac{1}{C_1}+\frac{1}{C_3}\right)-\frac{2}{C_1}\left(R_2R_3-\frac{L_2}{C_3}\right)\right)^2+4\left\{L_2R_3^2-L_2^2\left(\frac{1}{C_1}+\frac{1}{C_3}\right)\right\}\frac{1}{C_1C_3^2}}}{2\left\{L_2R_3^2-L_2^2\left(\frac{1}{C_1}+\frac{1}{C_3}\right)\right\}}\ \vdots}}{\sqrt{\frac{1}{L_2C_3+R_2R_3C_1C_3+\{L_2C_3+R_1C_1C_3(R_2+R_3)\}}}-\sqrt{\frac{R_1C_1-R_2C_1}{R_1C_1L_2C_3-R_3C_1L_2C_3}}} \tag{20}$$

5. MATLAB simulation results

The simulation results are presented as follows:

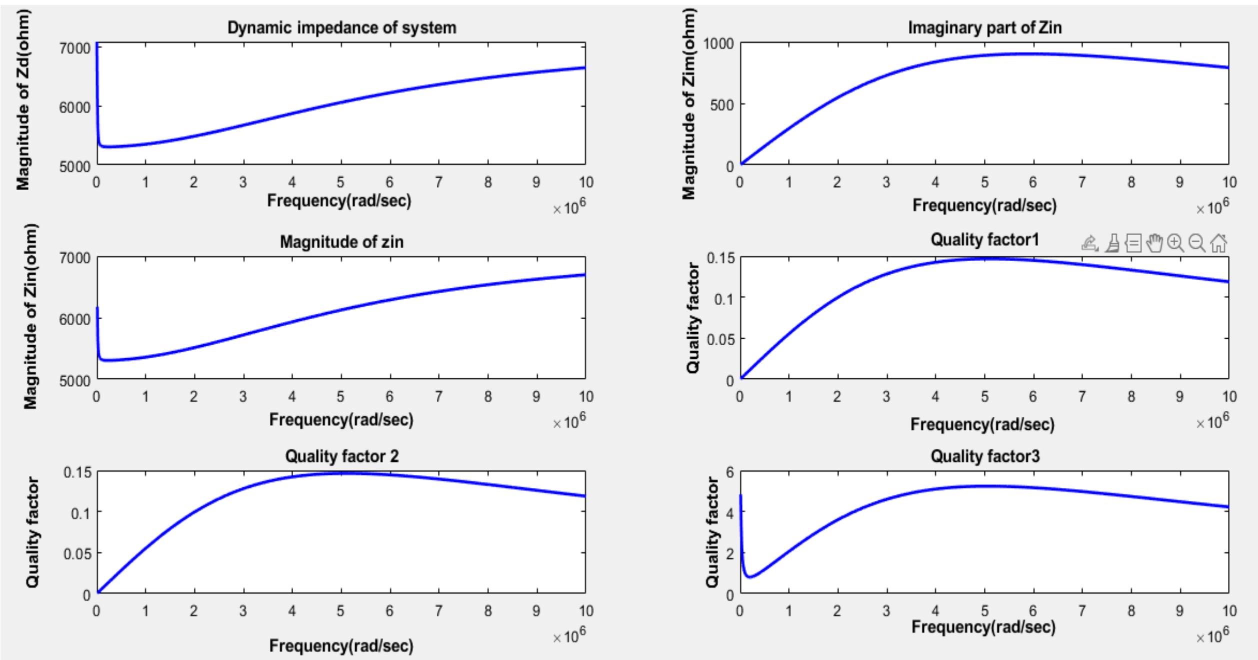

Figure 7. Simulated graph of all parameters of QA at $R_1 = 3530\ \Omega$, $R_2 = 3560\ \Omega$, and $R_3 = 3590\ \Omega$.

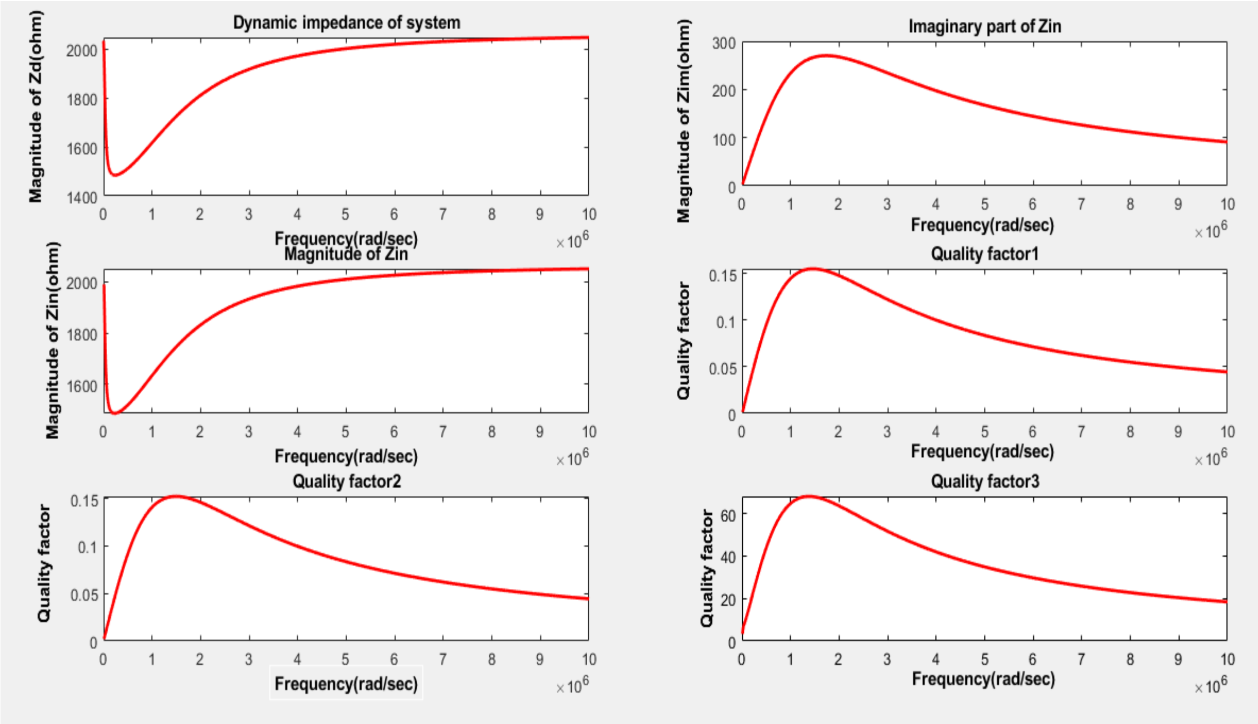

Figure 8. Simulated graph of all parameters of QA at $R_1 = 1000\ \Omega$, $R_2 = 1035\ \Omega$, and $R_3 = 1065\ \Omega$.

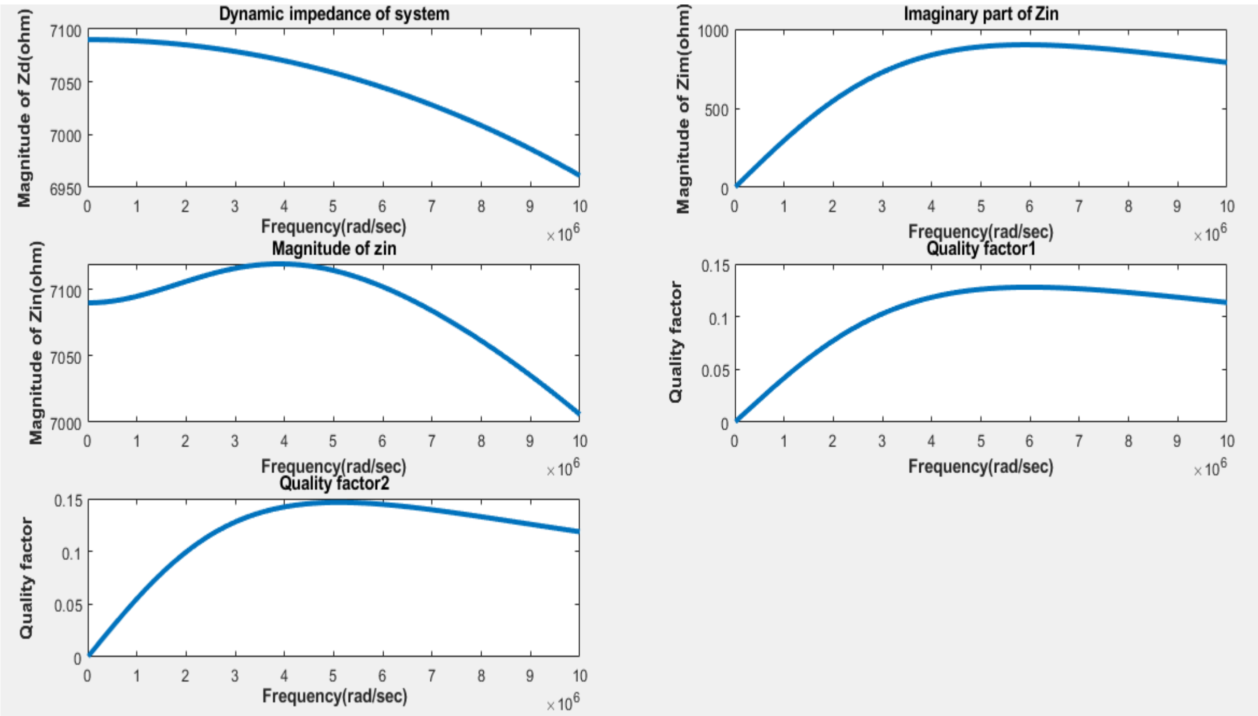

Figure 9. Simulated graph of all parameters of QA at $L_2 = 1210e - 6$H, $C_1 = 25e - 15$F, $C_3 = 143e - 15$F, $R_1 = 3530\ \Omega$, $R_2 = 3560\ \Omega$, and $R_3 = 3590\ \Omega$.

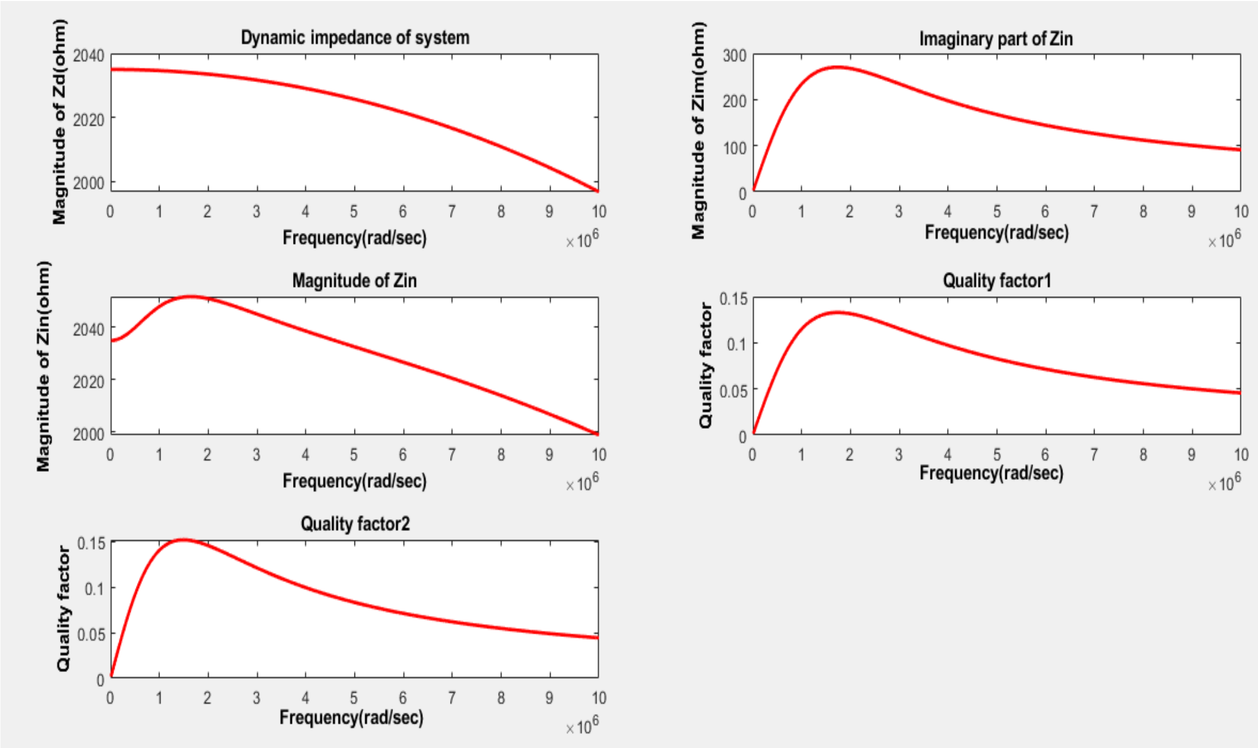

Figure 10. Simulated graph of all parameters of QA at L_2 = 1210e – 6H, C_1 = 25e – 15F, C_3 = 143e – 15F with R_1 = 1000 Ω, R_2 = 1035 Ω, and R_3 = 1065 Ω.

Figures 7–10 show the simulation plot of all parameters of QA at distinct values of L_2, C_1, C_3, R_1, R_2 and R_3.

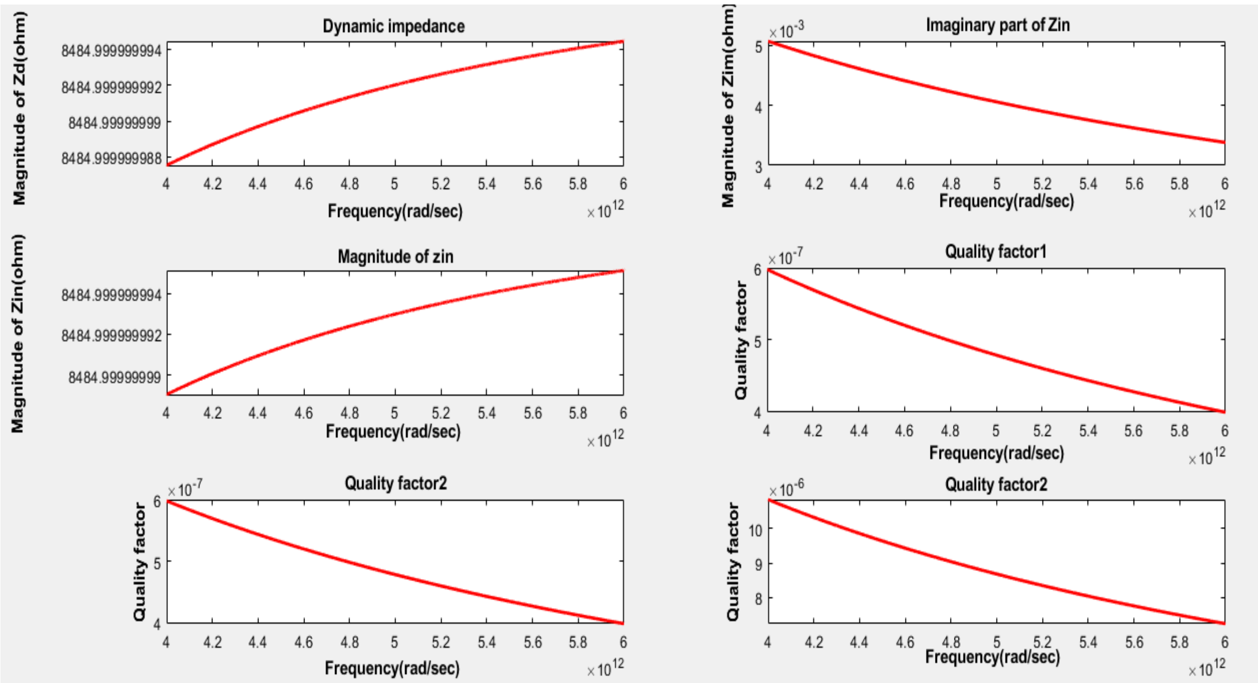

Figure 11. Simulated graph of all parameters of QA.

Table 2 indicates the approximate values of equivalent circuit parameters of QA at ω = 5 THz.

Table 2. Calculated values of circuit elements after synthesis of QA at 5 THz.

Frequency (THz)	The calculated value of QA circuit parameters					
ω	R_1 (kΩ)	R_2 (kΩ)	R_3 (kΩ)	L_2 (mH)	C_1 (μF)	C_3 (μF)
5	3.530	6.899	4.955	1210×10^{-3}	25×10^{-4}	143×10^{-4}

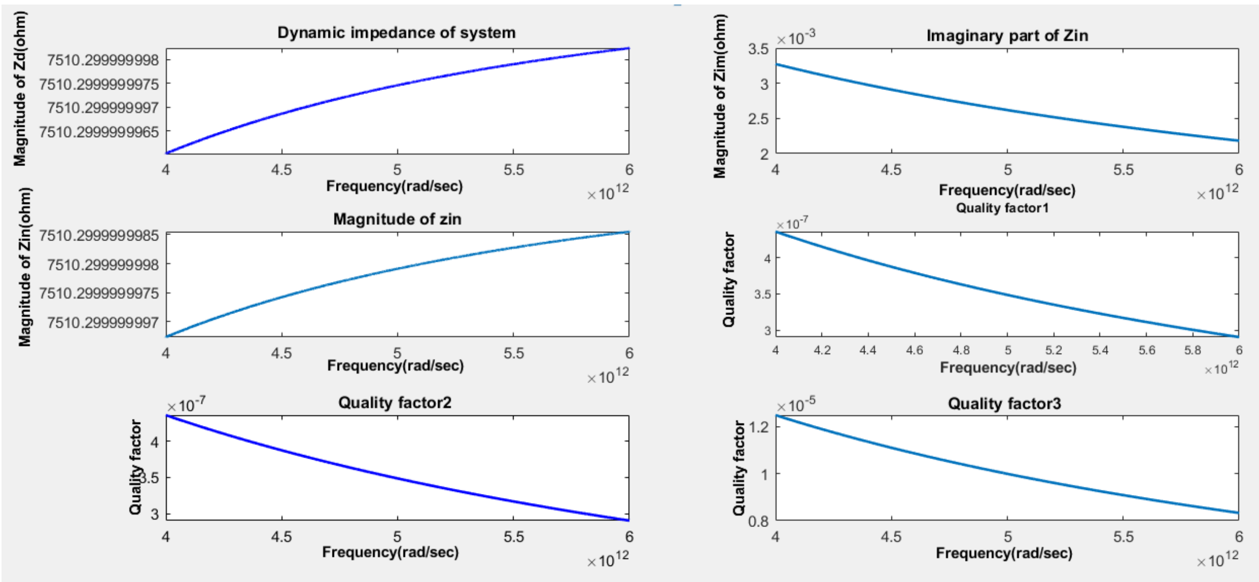

Figure 12. Simulated graph of all parameters of QA.

Table 3 represents the approximate values of equivalent circuit parameters of QA at ω = 10 THz.

Table 3. Evaluated values of QA circuit parameters after synthesis at 10 THz.

Frequency (THz)	The calculated value of QA circuit parameters					
ω	R_1 (kΩ)	R_2 (kΩ)	R_3 (kΩ)	L_2 (mH)	C_1 (μF)	C_3 (μF)
10	3.53	1.875	3.9803	1210×10^{-2}	25×10^{-4}	143×10^{-4}
10	3.53	3.881	4.131	1210×10^{-2}	129×10^{-4}	145×10^{-4}

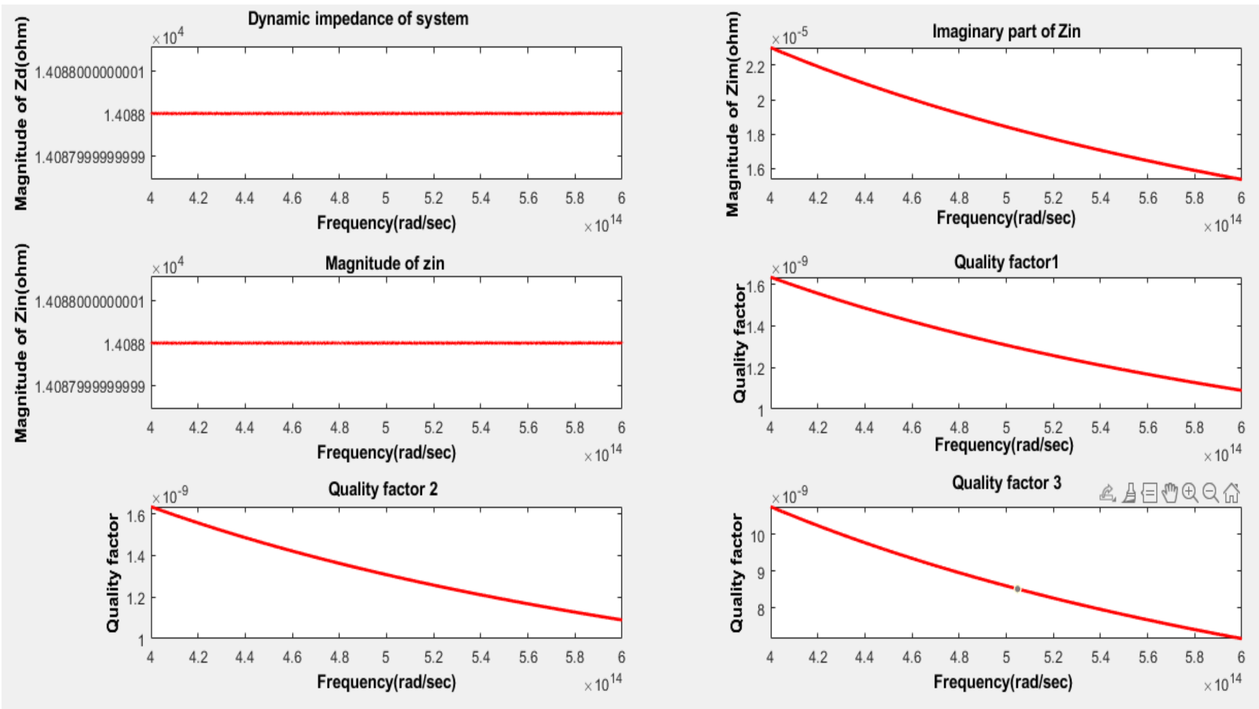

Figure 13. Simulated graph of all QA parameters.

Table 4 shows the approximate values of equivalent circuit parameters of QA at ω = 500 THz.

Table 4. Evaluated values of QA circuit parameters after synthesis at 500 THz.

Frequency (THz)	The calculated value of QA circuit parameters					
ω	R_1 (kΩ)	R_2 (kΩ)	R_3 (kΩ)	L_2 (mH)	C_1 (μF)	C_3 (μF)
500	3.53	9.999	10.558	1210×10^{-2}	129×10^{-4}	145×10^{-4}

$$f_r = \frac{c}{2\pi\sqrt{\epsilon_r}}\sqrt{\left(\frac{m\pi}{a}\right)^2 + \left(\frac{n\pi}{b}\right)^2 + \left(\frac{p\pi}{d}\right)^2}$$

From the study and analysis of **Figures 7–13**, it is clear that for a classical antenna, the frequency is generally in the GHz range but at the same time the dynamic impedance and its magnitude are also increased. Its effect the quality factor proportionally, so the bandwidth will be reduced. That's why such type of antenna has a limited range of signals while the nano DRA or quantum DRA operates at terahertz frequency due to which dynamic impedance decreases and magnitude of the impedance is also decreased that shows a decrement in quality factor but the increment in bandwidth. That's why such types of antenna are used for a wide range of signals. The mathematical analysis of quantum DRA in this article is a novel work that has not been presented in earlier studies.

The linear permittivity of a homogenous substance in free space is referred to as relative permittivity εr (also known as dielectric constant, although it is depreciated and refers to the static, zero frequency relative permittivity).

$Q = \frac{f_r}{f_h - f_l} = \frac{f_r}{\text{bandwidth}} = \frac{1}{\text{DF}} = \frac{X}{\text{ESR}} = \frac{1}{\tan\delta}$, equivalent series resistance (ESR).

6. Designing procedure and formulation of quantum DRA

Designing of quantum rectangular DRA

The perspective view of quantum rectangular DRA using HFSS is shown below:

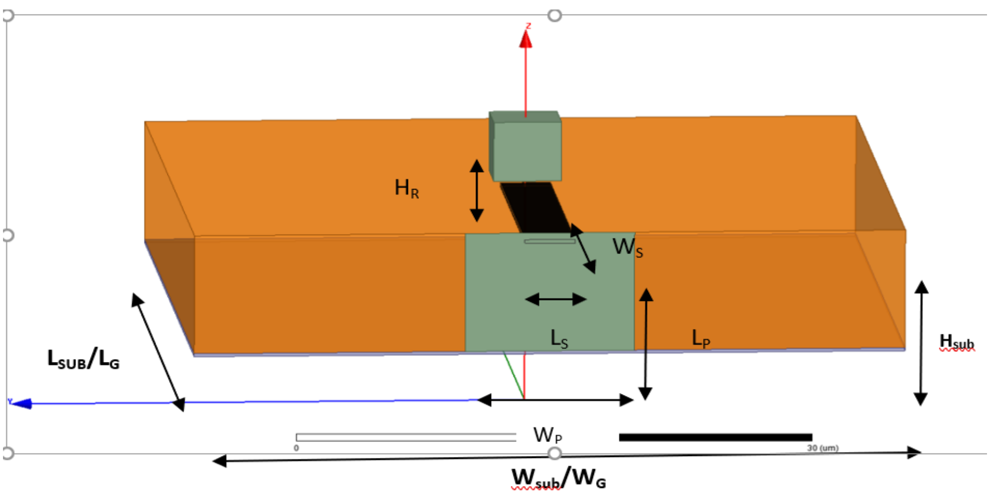

Figure 14. Quantum rectangular DRA.

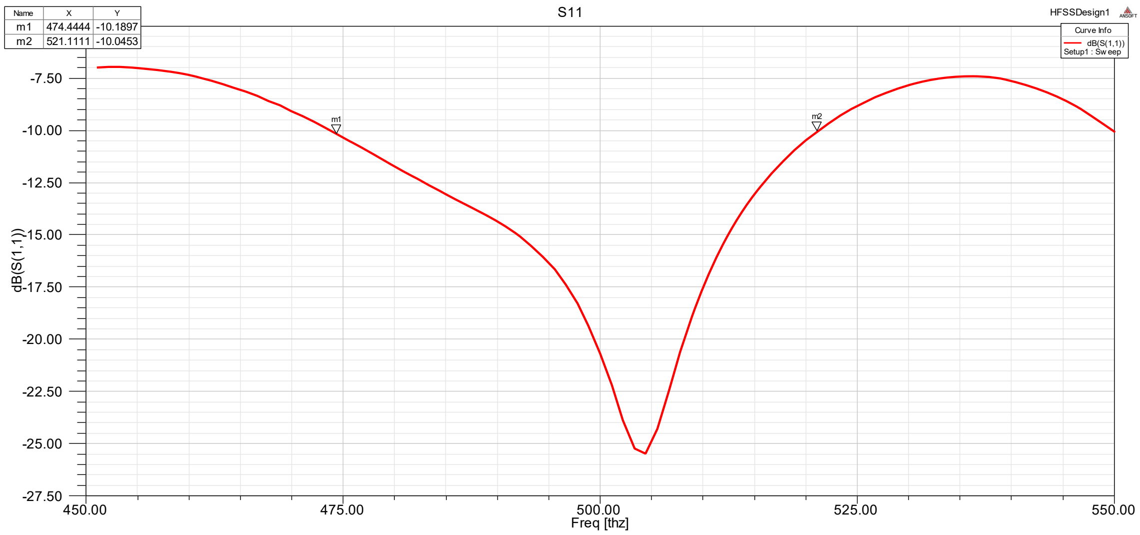

Figure 15. Simulated plot between reflection coefficient and frequency.

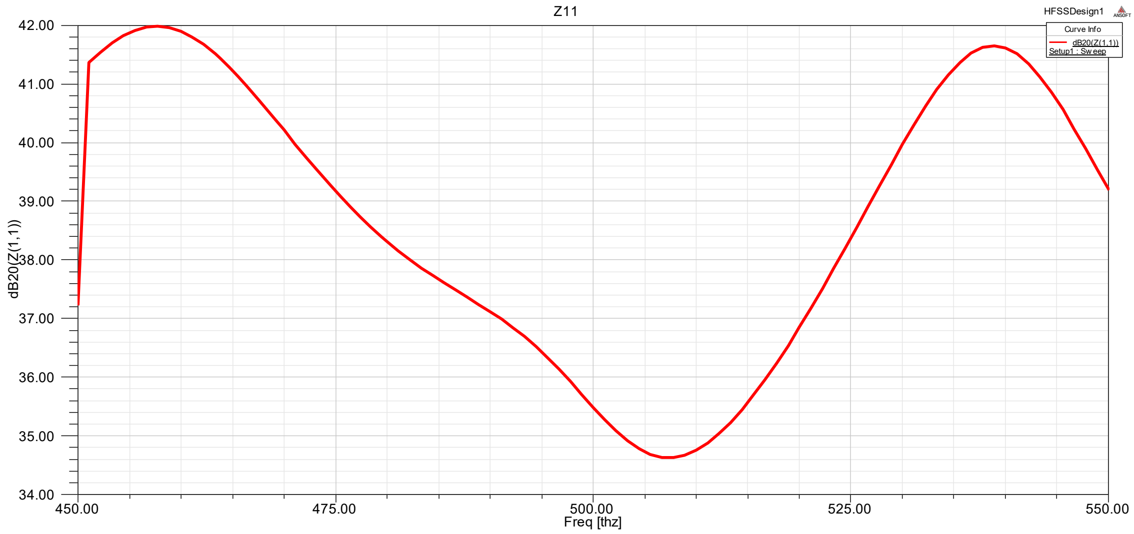

Figure 16. Simulated plot between input impedance and frequency.

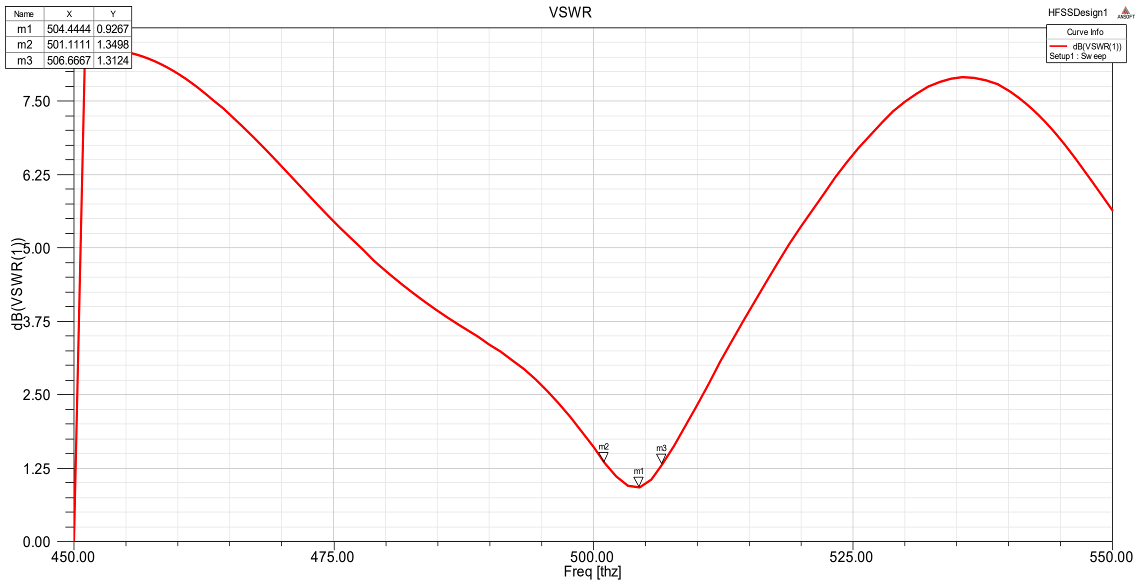

Figure 17. Simulated plot between VSWR and frequency.

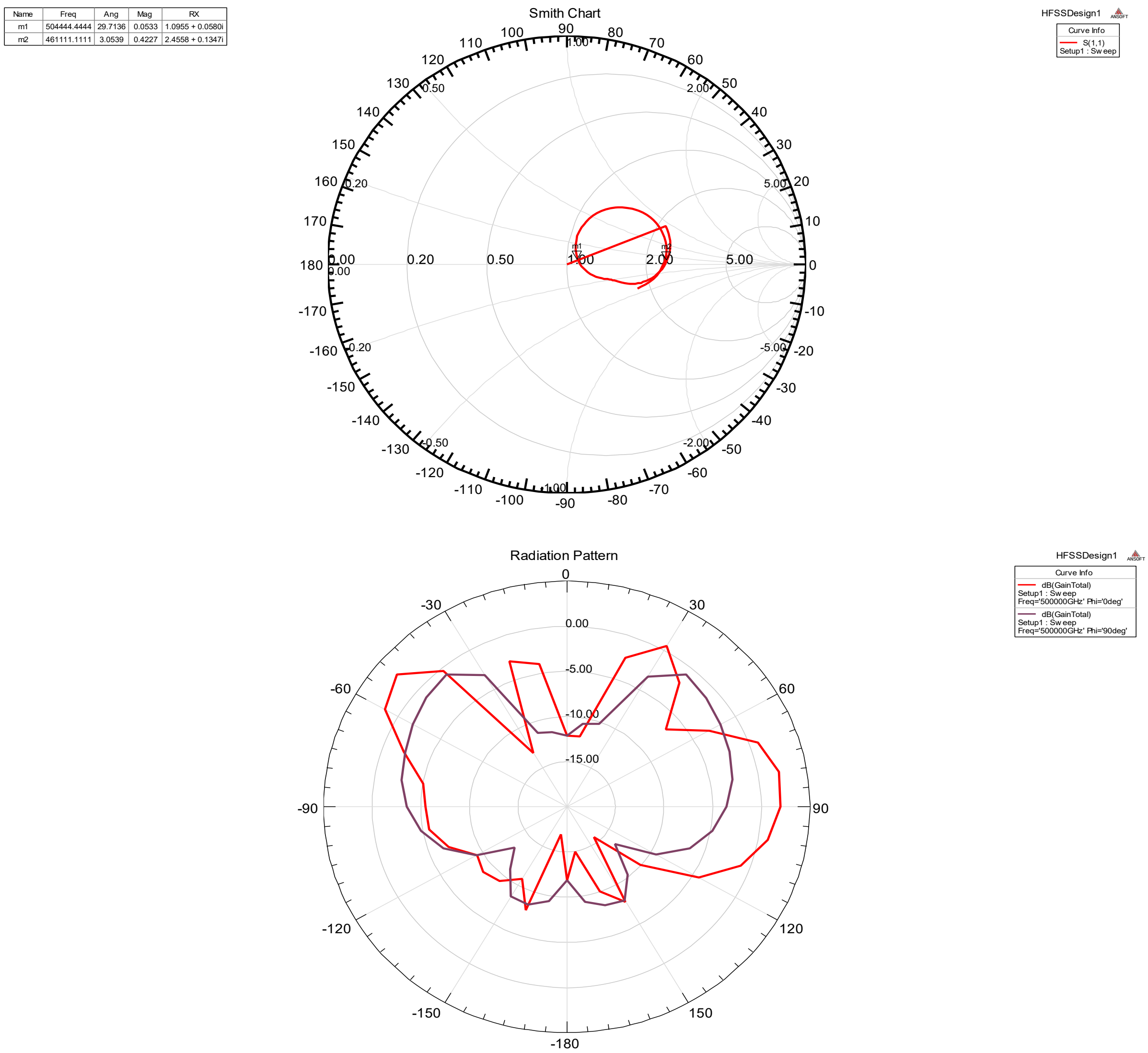

Figure 18. Radiation pattern quantum rectangular DRA.

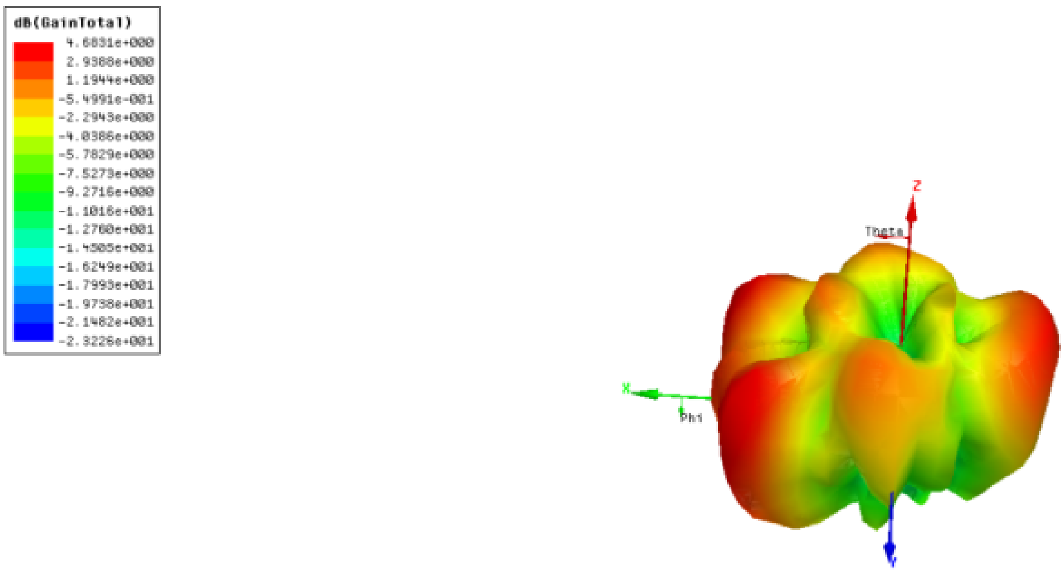

Figure 19. 3D polar plot quantum rectangular DRA.

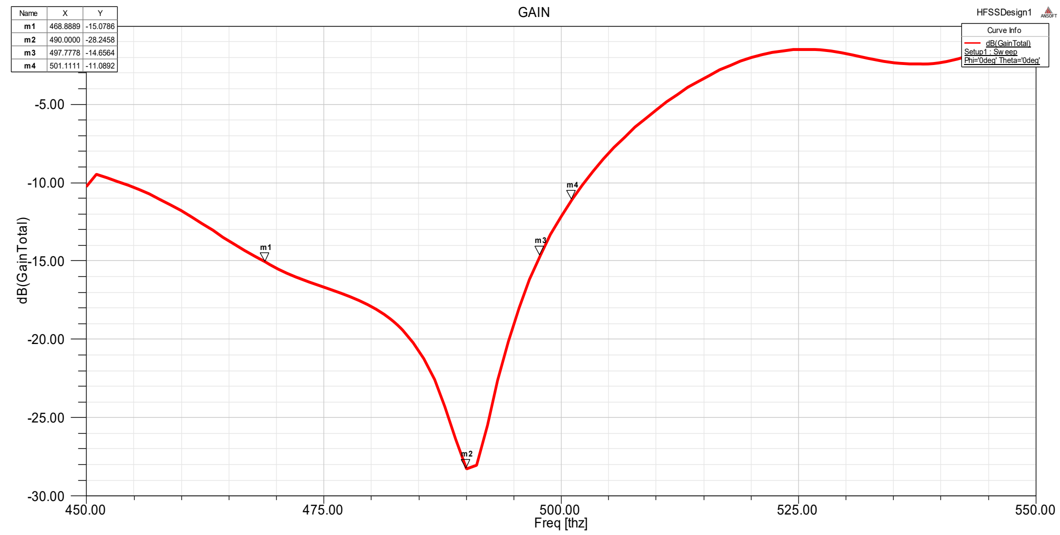

Figure 20. Simulated plot between gain and frequency.

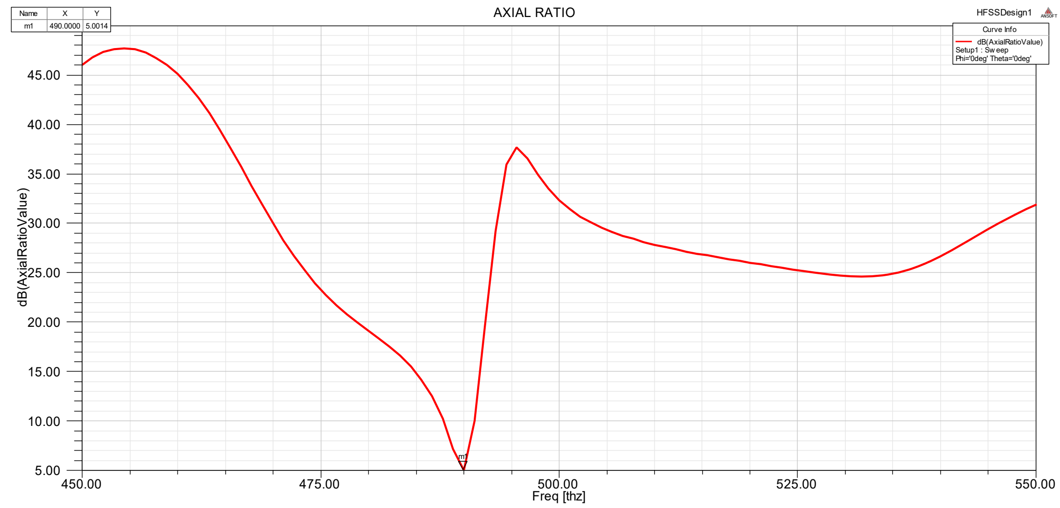

Figure 21. Simulated plot between axial ratio and frequency.

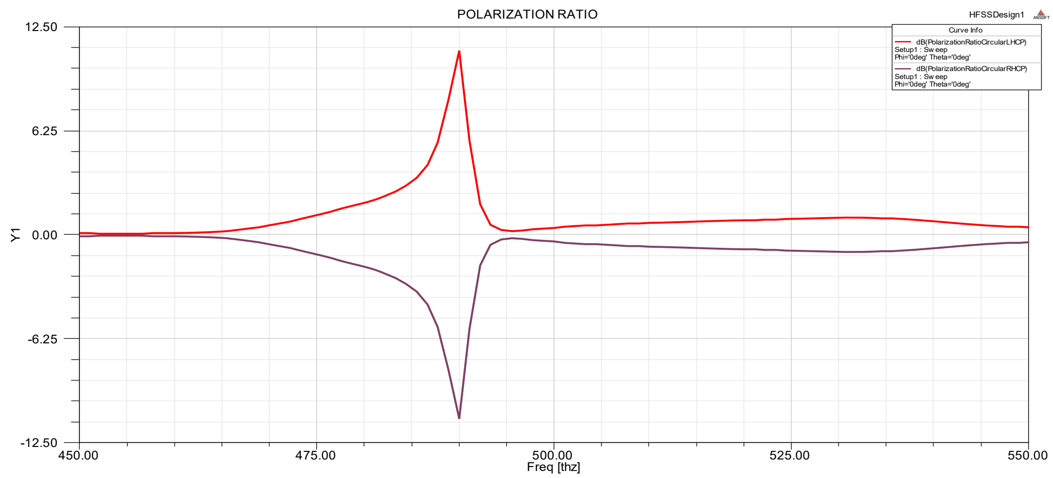

Figure 22. Simulated plot between polarization ratio and frequency.

The design, dimensions, and radiation pattern of THz rectangular DRAs, along with S_{11} Z_{11}, VSWR, and other antenna radiation patterns have been obtained in **Figures 14–18**. **Figures 19–22** show the graph of gain, axial ratio and polarization ratio versus frequency respectively. These can provide wider bandwidth and fast data rate. Terahertz DRA can be used for optical communication. It provides a new opportunity for fast communication systems. The equivalent circuit of terahertz DRA has already been explained in this article. For proper working of any antenna, the frequency must be less than −10 dB. The comparative study of proposed quantum DRA with respective to existing is shown in **Table 5**.

Table 5. Comparative study of proposed DRA with existing ones.

Authors	Title	Operating frequency /bandwidth
Pan et al.[50]	Compact quasi-isotropic dielectric resonator antenna with small ground plane	189 THz–194 THz
Kumar[51]	A compact graphene based nano-antenna for communication in nano-network	55 THz frequency with a peak gain of 5.47 dB
Kavitha et al.[52]	Graphene plasmonic nano-antenna for terahertz communication	30 THz frequency with a peak gain of 3.52 dB
Proposed nano DRA	Mathematical modeling and parameter analysis of quantum antenna for IoT sensor-based biomedical applications	511 THz frequency with good performance

7. Conclusion

In this paper, parameters like dynamic impedance (Z_d), quality factor, and input impedance (Z_{in}) of NDRA (QA) have been formulated and calculated by its electrical equivalent circuit that is a series and parallel sequence of resistor, inductor, and capacitor. The calculated and simulated results for different parameters are shown. Under tuning conditions, it has been ascertained that dynamic impedance is decreased with an increase in THz frequency (511 THz) which results in a decrement in power losses, therefore it requires less power for signal transmission. Due to low power dissipation, there is low-temperature variation, and due to this less number of body tissues are damaged when used in biomedical applications just like laser operation. The integration of IoT technology with quantum antennas has the potential to significantly improve the performance and efficiency of wireless communication systems. Therefore, this research article on NDRA (QA) circuits can facilitate developers in sensible realization for bioscience and medical applications and the results have been validated at 5 THz, 10 THz and 500 THz. Quantum antenna is very high bandwidth and high dissipation factor (D.F), can be used for sensors and wide band antennas for high-speed communications applications. Simulation results based on optical DRAs have been included along with equivalent R, L, C circuit and MATLAB based mathematical analysis.

Author contributions

Conceptualization, RK (Ram Krishna) and RSY; methodology, RK (Ram Krishna); software, RK (Ram Krishna) and RK (Ravinder Kumar); validation, RK (Ram Krishna), RSY and HS; formal analysis, RK (Ram Krishna); investigation, RK (Ram Krishna); resources, RK (Ram Krishna) and AKR; data curation, RK (Ram Krishna); writing—original draft preparation, RK (Ram Krishna) and HS; writing—review and editing, RK (Ram Krishna) and HS; visualization, RK (Ram Krishna); supervision, RSY; project administration, RK (Ram Krishna), RSY and NG; funding acquisition, AKR and RK (Ram Krishna). All authors have read and agreed to the published version of the manuscript.

Conflict of interest

The authors declare no conflict of interest.

References

1. Alam M, Massoud Y. RLC ladder model for scattering in single metallic nanoparticles. *IEEE Transactions on Nanotechnology* 2006; 5(5): 491–498. doi: 10.1109/TNANO.2006.880403

2. Ahmad R, Farooqi A, Farooqi R, et al. A new fractional-order stability analysis of sir model for the transmission of Buruli disease: A biomedical application. *Fractals* 2022; 30(5): 1–11. doi: 10.1142/S0218348X22401715
3. Ambrosio LA, Hernández-Figueroa HE. RLC circuit model for the scattering of light by small negative refractive index spheres. *IEEE Transactions on Nanotechnology* 2012; 11(6): 1217–1222. doi: 10.1109/TNANO.2012.2221739
4. Tzarouchis DC, Ylä-Oijala P, Sihvola A. Resonant scattering characteristics of homogeneous dielectric sphere. *IEEE Transactions on Antennas and Propagation* 2017; 65(6): 3184–3191. doi: 10.1109/TAP.2017.2690312
5. Mongia RK, Bhartia P. Dielectric resonator antennas—A review and general design relations for resonant frequency and bandwidth. *International Journal of RF and Microwave Computer-Aided Engineering* 1994; 4(3): 230–247. doi: 10.1002/mmce.4570040304
6. Alam M, Massoud Y. An accurate closed-form analytical model of single nanoshells for cancer treatment. In: Proceedings of 48th Midwest Symposium on Circuits and Systems; 7–10 August 2005; Covington, America. pp. 1928–1931.
7. Oubre C, Nordlander P. Optical properties of metallodielectric nano structures calculate using the finite difference time domain method. *The Journal of Physical Chemistry B* 2004; 108(46): 17740–17747. doi: 10.1021/jp0473164
8. Alam M, Massoud Y. A closed-form analytical model for single nanoshells. *IEEE Transactions on Nanotechnology* 2006; 5(3): 265–272. doi: 10.1109/TNANO.2006.874050
9. Li JLW, Li Z, She H, et al. A new closed-form solution to light scattering by spherical nanoshells. *IEEE Transactions on Nanotechnology* 2009; 8(5): 617–626. doi: 10.1109/TNANO.2009.2021696
10. Farhat M, Rockstuhl C, Bağcı H. A 3D tunable and multi-frequency graphene plasmonic cloak. *Optics Express* 2013; 21(10): 12592–12603. doi: 10.1364/OE.21.012592
11. Ghadarghadr S, Mosallaei H. Coupled dielectric nanoparticles manipulating metamaterials optical characteristics. *IEEE Transactions on Nanotechnology* 2009; 8(5): 582–594. doi: 10.1109/TNANO.2009.2013619
12. Ahmad R, Farooqi A, Zhang J, Ali N. Steady flow of a power law fluid through a tapered non-symmetric stenotic tube. *Applied Mathematics and Nonlinear Sciences* 2019; 4(1): 255–266. doi: 10.2478/AMNS.2019.1.00022
13. Khandelwal MK, Kanaujia BK, Kumar S. Defected ground structure: Fundamentals, analysis, and applications in modern wireless trends. *International Journal of Antennas and Propagation* 2017; 2017(1): 1–22. doi: 10.1155/2017/2018527
14. Vakil A. Transformation Optics Using Graphene: One-atom-thick Optical Devices Based on Graphene [PhD thesis]. University of Pennsylvania; 2012.
15. Christensen T, Jauho AP, Wubs M, Mortensen NA. Localized plasmons in graphene-coated nanospheres. *Physical Review B* 2015; 91(12): 125414. doi: 10.1103/PhysRevB.91.125414
16. Abramowitz M, Stegun IA. *Handbook of Mathematical Functions: With formulas, Graphs, and Mathematical Tables*. Courier Corporation; 1964.
17. Novotny L, Hecht B. *Principles of Nano-optics*. Cambridge University Press; 2006.
18. Farooqi A, Ahmad R, Alotaibi H, et al. A comparative epidemiological stability analysis of predictor corrector types non-standard finite difference scheme for the transmissibility of measles. *Results in Physics* 2021; 21: 103756. doi: 10.1016/j.rinp.2020.103756
19. Kroto HW, Heath JR, O'Brien SC, et al. C_{60}: Buckminsterfullerene. *Nature* 1985; 318: 162–163.
20. Yang H, Hou Z, Zhou N, et al. Graphene encapsulated SnO_2 hollow spheres as high-performance anode materials for lithiumion batteries. *Ceramics International* 2014; 40(9): 13903–13910. doi: 10.1016/j.ceramint.2014.05.109
21. Lee JS, Kim SI, Yoon JC, Jang JH. Chemical vapor deposition of mesoporous graphene nanoballs for supercapacitor. *ACS Nano* 2013; 7(7): 6047–6055. doi: 10.1021/nn401850z
22. Naserpour M, Zapata-Rodríguez CJ, Vuković SM, et al. Tunable invisibility cloaking by using isolated graphene coated nanowires and dimers. *Scientific Reports* 2017; 7(1): 12186. doi: 10.1038/s41598-017-12413-4
23. Biagioni P, Huang JS, Hecht B. Nanoantennas for visible and infrared radiation. *Reports on Progress in Physics* 2012; 75(2): 024402. doi: 10.1088/0034-4885/75/2/024402
24. Zou L, Withayachumnankul W, Shah CM, et al. Dielectric resonator nanoantennas at visible frequencies. *Optics Express* 2013; 21(1): 1344–1352. doi: 10.1364/OE.21.001344
25. Malheiros-Silveira GN, Wiederhecker GS, Hernández-Figueroa HE. Dielectric resonator antenna for applications in nanophotonics. *Optics Express* 2013; 21(1): 1234–1239. doi: 10.1364/OE.21.001234
26. Zhao Y, Engheta N, Alù A. Effects of shape and loading of optical nanoantennas on their sensitivity and radiation properties. *Journal of the Optical Society of America B* 2011; 28(5): 1266–1274. doi: 10.1364/JOSAB.28.001266

27. Alam M, Massoud Y. An accurate closed-form analytical model of single nanoshells for cancer treatment. *IEEE International Midwest Symp, Circuits System* 2005; 2(1): 1928–1931. doi: 10.1109/mwscas.2005.1594503
28. Yaduvanshi RS, Parthasarathy H. Coupled solution of Boltzmann transport equation, Maxwell's and Navier Stokes equations. *International Journal for Infonomics* 2010; 3(4): 422–428. doi: 10.20533/iji.1742.4712.2010.0046
29. Zou L, Withayachumnankul W, Shah CM, et al. Efficiency and scalability of dielectric resonator antennas at optical frequencies. *IEEE Photonics Journal* 2014; 6(4): 1–10. doi: 10.1109/JPHOT.2014.2337891
30. Yaduvanshi RS, Varshney G. *Nano Dielectric Resonator Antennas for 5G Applications*, 1st ed. CRC Press; 2020.
31. Kumar A, Yaduvanshi RS. Quantum antenna operating at 430 to 750 THz band, inspired through human eye. *Journal of Information and Optimization Sciences* 2020; 41(6): 1365–1373. doi: 10.1080/02522667.2020.1809093
32. Kumar SB, Singhal PK. RF energy harvesting using Sierpinski's gasket fractal antenna with EBG geometry. *Journal of Information and Optimization Sciences* 2020; 41(1): 99–106. doi: 10.1080/02522667.2020.1715561
33. Krishna R, Imoize AL, Yaduvanshi RS, et al. Analysis of multi-stacked dielectric resonator antenna with its equivalent R-L-C circuit modeling for wireless communication systems. *Mathematical and Computational Applications* 2022; 28(1): 4. doi: 10.3390/mca28010004
34. Yadav R, Katiyar S, Yaduvanshi RS, et al. Analysis of dielectric resonator antenna with its equivalent R, L, C circuit modelling, *Journal of Information and Optimization Sciences* 2020; 41(6): 1375–1393. doi: 10.1080/02522667.2020.1822043
35. Ratan R, Singh H, Srivastava A, Luthra SK. Designing of fuzzy knowledge-based controller (FKBC) for optical communication system. *International Journal of Engineering Research & Technology* 2013; 6(8): 5–8.
36. Yaduvanshi RS, Yadav RK, Katiyar S, et al. Optical spherical dielectric resonator antenna for sensing and wireless communication. *Frequenz* 2020; 75(1–2): 49–59. doi: 10.1515/freq-2020-0086
37. Kumar A, Sharma S, Goyal N, et al. Energy-efficient fog computing in internet of things based on routing protocol for low-power and lossy network with Contiki. *International Journal of Communication Systems* 2022; 35(4): e5049. doi: 10.1002/dac.5049
38. Singh H, Solanki RS. Classification & feature extraction of brain tumor from MRI images using modified ANN approach. *International Journal of Electrical and Electronics Research* 2021; 9(2): 10–15. doi: 10.37391/IJEER.090202
39. Rana SK, Rana SK, Nisar K, et al. Blockchain technology and artificial intelligence based decentralized access control model to enable secure interoperability for healthcare. *Sustainability* 2022; 14(15): 9471. doi: 10.3390/su14159471
40. Rana AK, Sharma S. Enhanced energy-efficient heterogeneous routing protocols in WSNs for IoT application. *International Journal of Engineering and Advanced Technology* 2019; 9(1): 4418–4425. doi: 10.35940/ijeat. A1342.109119
41. Rana AK, Sharma S. Industry 4.0 manufacturing based on IoT, cloud computing, and big data: Manufacturing purpose scenario. In: Hura GS, Kumar SA, Siong HL (editors). *Advances in Communication and Computational Technology*. Springer; 2021. pp. 1109–1119.
42. Rana AK, Sharma S. Contiki cooja security solution (CCSS) with IPv6 routing protocol for low-power and lossy networks (RPL) in internet of things applications. In: Marriwala N, Tripathi CC, Kumar D, Jain S (editors). *Mobile Radio Communications and 5G Networks*. Springer; 2020. pp. 251–259.
43. Kumar A, Sharma S. IFTTT rely based a semantic web approach to simplifying trigger-action programming for end-user application with IoT applications. In: Pandey R, Paprzycki M, Srivastava N, et al (editors). *Semantic IoT: Theory and Applications*. Springer; 2021. pp. 385–397.
44. Kumar A, Sharma S. Internet of things (IoT) with energy sector-challenges and development. In: *Electrical and Electronic Devices, Circuits and Materials: Design and Applications*. CRC Press; 2021. pp. 183.
45. Kumar A, Sharma S, Dhawan S, et al. E-learning with Internet of things. In: Goyal N, Sharma S, Rana AK, Tripathi SL (editors). *Internet of Things: Robotic and Drone Technology*. CRC Press; 2022. pp. 195.
46. Rana AK, Sharma S. The fusion of blockchain and IoT technologies with industry 4.0. In: Sharma K, Gupta A, Sharma B, Tripathi SL (editors). *Intelligent Communication and Automation Systems*. CRC Press; 2021. pp. 275–290.
47. Rana AK, Sharma S, Dhawan S, Tayal S. Towards secure deployment on the Internet of robotic things: Architecture, applications, and challenges. In: Gupta R, Khari M (editors). *Multimodal Biometric Systems*. CRC Press; 2021. pp. 135–148.
48. Arora S, Sharma S, Rana AK. Ultrawide band antenna for wireless communications. In: Goyal N, Sharma S, Kumar Rana A, Tripathi SL (editors). *Internet of Things: Robotic and Drone Technology*. CRC Press; 2022. pp. 95.

49. Kumar A, Sharma S. Demur and routing protocols with application in underwater wireless sensor networks for smart city. In: Goyal N, Gupta R, Khari M (editors). *Energy-efficient Underwater Wireless Communications and Networking*. IGI Global; 2020. pp. 262–278.
50. Pan YM, Leung KW, Lu K. Compact quasi-isotropic dielectric resonator antenna with small ground plane. *IEEE Transactions on Antennas and Propagation* 2013; 62(2): 577–585. doi: 10.1109/TAP.2013.2292082
51. Kumar MR. A compact graphene based nano-antenna for communication in nano-network. *Journal of the Institute of Electronics and Computer* 2019; 1: 17–27. doi: 10.33969/JIEC.2019.11003
52. Kavitha S, Sairam K, Singh A. Graphene plasmonic nano-antenna for terahertz communication. *SN Applied Sciences* 2022; 4: 114. doi: 10.1007/s42452-022-04986-1